



Defence Research and
Development Canada

Recherche et développement
pour la défense Canada



Technical Description of Urban Microscale Modeling System: Component 1 of CRTI Project 02-0093RD

E. Yee
DRDC Suffield

F.S. Lien and H. Ji
Waterloo CFD Engineering Consulting Inc.

Technical Report
DRDC Suffield TR 2007-067
March 2007

DISTRIBUTION STATEMENT A
Approved for Public Release
Distribution Unlimited

Canada

Technical Description of Urban Microscale Modeling System: Component 1 of CRTI Project 02-0093RD

Eugene Yee
Defence R&D Canada – Suffield

Fue-Sang Lien and Hua Ji
Waterloo CFD Engineering Consulting, Inc.

20071002079

Defence R&D Canada – Suffield

Technical Report

DRDC Suffield TR 2007-067

March 2007

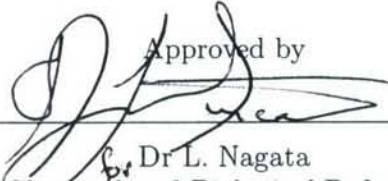
AQ F07-12-13503

Author



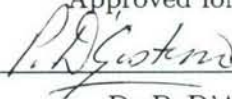
Eugene Yee

Approved by



Dr L. Nagata
Head, Chemical and Biological Defence Section

Approved for release by



Dr P. D'Agostino
Chair, DRDC Suffield DRP

Abstract

This report provides a technical description of the models that comprise Component 1 of a 4-year Chemical, Biological, Radiological and Nuclear Research and Technology Initiative (CRTI) Project 02-0093RD entitled "An Advanced Emergency Response System for Chemical Biological Radiological and Nuclear (CBRN) Hazard Prediction and Assessment for the Urban Environment" whose primary objective is the development of an advanced, fully validated, state-of-the-science modeling system for the prediction of urban flow (i.e., turbulent flow through cities) and the concomitant problem of modeling the dispersion of CBRN agents released in a populated urban environment. The principal module of Component 1 is urbanSTREAM, which is a general second-order accurate finite-volume code designed for the simulation of urban flow using a two-equation turbulence closure model (namely, the standard k - ϵ model and the limited-length-scale k - ϵ model). Component 1 also incorporates a module (urbanGRID) for the automatic generation of grids in the computational domain when provided with detailed geometric information on the shapes and locations of buildings in the urban environment in the form of Environmental Systems Research Institute (ESRI) Shapefiles. Finally, Component 1 also includes modules for the prediction of urban dispersion in the Eulerian framework: namely, urbanEU which is an Eulerian grid dispersion model based on numerical solution of a K -theory advection-diffusion equation (source-oriented approach) and urbanAEU which is a receptor-oriented dispersion model based on numerical solution of the adjoint of the K -theory advection-diffusion equation. The report describes the current status of the urban microscale flow and dispersion modeling system developed in Component 1 and presents a case study of the application of this system in stand-alone mode to the simulation of flow and tracer dispersion in a real cityscape. The numerical simulations of Intensive Observation Period (IOP) 9 in the Joint Urban 2003 (JU2003) experiments conducted in Oklahoma City, Oklahoma provide an initial demonstration that the developed modeling system can correctly reproduce many features of the flow and dispersion in a real urban environment.

Résumé

Ce rapport fournit une description technique des modèles compris dans la Composante 1 d'un projet de 4 ans appelé Initiative de recherche et de technologie chimique, biologique, radiologique et nucléaire (IRTC), Projet 02-0093RD intitulé "Système amélioré d'intervention d'urgence de prédiction de dangers chimiques, biologiques, radiologiques et nucléaires (CBRN) et d'Évaluation du milieu urbain". L'objectif principal de ce projet consiste à développer un système de modélisation, à la pointe de la recherche scientifique et totalement validé, de prédiction du courant urbain (ex. : courant turbulent à travers les villes) ainsi que du problème concomitant de la modélisation de la dispersion des agents CBRN lâchés dans le milieu urbain peuplé. Le module principal de la Composante 1 est urbanSTREAM, un code général de deuxième ordre de volume fini exact conçu pour simuler le courant urbain en utilisant un schéma de fermeture de turbulence à deux équations (dont le schéma $k-\epsilon$ et le schéma $k-\epsilon$ d'échelle de longueur limitée). La composante 1 incorpore aussi un module (urbanGRID) pour la génération automatique de grilles dans le domaine computationnel quand sont fournies les informations géométriques détaillées des formes et des emplacements des bâtiments du milieu urbain sous forme de Fichiers de formes provenant de l'institut Environmental Systems Research Institute (ESRI). Enfin, la composante 1 comprend aussi des modules de prédiction de la dispersion urbaine dans le cadre conceptuel eulérien, dont urbanEU qui est un modèle de dispersion de grille eulérienne, basé sur la solution numérique d'une équation advection-diffusion de la théorie K (méthode axée sur la source) et urbanAEU qui est un modèle de dispersion axé sur les récepteurs, basé sur une solution numérique de l'adjoint de l'équation advection-diffusion de la théorie K. Ce rapport décrit le statut actuel du système de courants urbains à micro-échelle et de modélisation de la dispersion dans la Composante 1 et présente une étude de cas de l'application de ce système, en mode autonome, à la simulation des courants et de la dispersion des traceurs dans un paysage urbain réel. Les simulations numériques de la Période d'observation intensive (POI) 9 des expériences Joint Urban 2003 (JU2003), conduites à Oklahoma City en Oklahoma, commencent à démontrer que le système de modélisation mis au point a la capacité de reproduire correctement beaucoup de caractéristiques des courants et de dispersion dans un milieu urbain réel.

Executive summary

Introduction: The release of chemical, biological, or radiological (CBR) agents by terrorists or rogue states in a North American city (densely populated urban center) and the subsequent exposure, deposition, and contamination are emerging threats in an uncertain world. As a consequence, the understanding of the wind flow in an urban area and the concomitant dispersion of material released into that flow is crucially important. Unfortunately, predictive models for urban flow and dispersion do not exist. In view of this, the work described in this report was undertaken to address this important capability gap.

Results: This report provides a technical description of the models that comprise Component 1 of a 4-year Chemical, Biological, Radiological and Nuclear Research and Technology Initiative (CRTI) Project 02-0093RD. This project entitled "An Advanced Emergency Response System for Chemical Biological Radiological and Nuclear (CBRN) Hazard Prediction and Assessment for the Urban Environment" involved a collaborative model development effort by Defence R&D Canada – Suffield and Environment Canada. The primary objective of the project was to develop an advanced, fully validated, state-of-the-science modeling system for the prediction of urban flow and for the modeling of the dispersion of CBRN agents released in these flows. Defence R&D Canada – Suffield was responsible for Component 1 of CRTI Project 02-0093RD which involved (1) development and implementation of a computational fluid dynamics model for the simulation of urban flow in an arbitrary cityscape; (2) development of a grid generation capability for the automatic generation of grids in the computational domain when provided with detailed geometric information on the shapes and locations of buildings; (3) provision of predictive models for urban dispersion; and, (4) validation of all these model components. The report provides a detailed technical description of the urban flow and dispersion models developed for CRTI-02-0093RD and presents a case study of the application of these models to the simulation of flow and contaminant dispersion in a real cityscape. The numerical simulations of Intensive Observation Period (IOP) 9 in the Joint Urban 2003 (JU2003) experiments conducted in Oklahoma City, Oklahoma provide an initial demonstration that the developed modeling capability can correctly reproduce many features of the flow and dispersion in a real urban environment.

Significance and Future Plans: The availability of high-fidelity, time-dependent models for the prediction of a CBR agent's movement and fate in a complex urban environment will provide the strongest technical and scientific foundation for support of Canada's more broadly based effort at advancing counter-terrorism planning and operational capabilities. The final product of this research and development effort will be a high-fidelity multi-scale CBR modeling system that will be fully operational at the Environmental Emergency Response Division (EERD) at the Canadian Meteorological Centre (CMC). This resource will serve as a nation-wide general problem-solving tool for first-responders involved with CBR incidents in the urban environment and beyond. Future plans for the modeling system described here include: (1) incorporation of more advanced turbulence models for prediction of complex flows; (2) inclusion of thermal effects; and, (3) inclusion of an adaptive mesh refinement capability (among others).

Yee, E., Lien, F.S. and Ji, H. (2007). Technical Description of Urban Microscale Modeling System: Component 1 of CRTI Project 02-0093RD. (DRDC Suffield TR 2007-067). Defence R&D Canada – Suffield.

Sommaire

Introduction: La libération d'agents chimiques, biologiques ou radiologiques (CBR) par des terroristes ou des états sans scrupules, dans une ville nord-américaine (centre urbain peuplé densément) et l'exposition, dépôt et contamination atmosphériques qui s'en suivraient sont les menaces émergentes d'un monde incertain. En conséquence, la compréhension des courants venteux dans une zone urbaine et de la dispersion concomitante des matières libérées dans ces courants est très importante. Les modèles de prédiction des courants urbains et de dispersion n'existent malheureusement pas. De ce fait, les travaux décrits dans ce rapport ont été entrepris pour aborder le problème de cette importante lacune.

Résultats: Ce rapport fournit une description technique des modèles compris dans la Composante 1 d'un projet de 4 ans appelé Initiative de recherche et de technologie chimique, biologique, radiologique et nucléaire (IRTC), Projet 02-0093RD. Ce projet intitulé "Système amélioré d'intervention d'urgence de prédiction de dangers chimiques, biologiques, radiologiques et nucléaires (CBRN) et d'Évaluation du milieu urbain" consiste en un effort collaboratif de développement de modèle entre R&D pour la défense Canada - Suffield et Environnement Canada. L'objectif principal consistait à développer un système de modélisation, à la pointe de la recherche scientifique et totalement validé, de prédiction des courants urbains et à modéliser la dispersion d'agents CBRN libérés dans ces courants. R&D pour la défense Canada - Suffield était chargé de la Composante 1 du Projet Project 02-0093RD de IRTC comprenant (1) le développement et l'implémentation du modèle de calcul de la dynamique des fluides pour la simulation des courants urbains dans un paysage urbain arbitraire; (2) le développement d'une capacité à générer des grilles pour la génération automatique de grilles dans le domaine computationnel quand sont fournis les renseignements géométriques détaillés des formes et des emplacements des bâtiments; (3) la provision de modèles de prédiction de la dispersion urbaine; (4) la validation de toutes les composantes de ces modèles. Le rapport procure une description technique détaillée des courants et des modèles de dispersion urbains développés pour IRTC-02-0093RD et présente un étude de cas pour l'application de ces modèles de simulation des courants et de la dispersion des contaminants dans un paysage urbain réel. Les simulations numériques de la Période d'observation intensive (POI) 9 dans les expériences Joint Urban 2003 (JU2003) conduites à Oklahoma City en Oklahoma, commencent à démontrer que les capacités de modélisation mises au point sont capables de reproduire correctement beaucoup de caractéristiques des courants et de dispersion dans un milieu urbain réel.

Portée des Résultats et les Plans Futurs: La disponibilité de modèles de haute fidélité et dépendants du temps, concernant la prédiction du mouvement et du sort des agents CBR dans un milieu urbain complexe, procurera les fondements techniques et scientifiques les plus solides en soutien aux efforts plus généraux du Canada à améliorer la planification du contreterrorisme et de ses capacités opérationnelles. Le produit final de cet effort en recherche et développement consistera en un système de modélisation CBR à multi échelle et de haute fidélité qui sera totalement opérationnel à la Division de la réponse aux urgences environnementales du Centre Météorologique Canadien (CMC). Cette ressource servira d'outil de résolution de problèmes généraux, à l'échelle de la nation, aux premiers intervenants participant aux incidents CBR, dans le milieu urbain et au-delà. Les plans futurs du système de modélisation d'écrit ici comprend: (1) l'incorporation de modèles améliorés de turbulences pour la prédiction des courants complexes; (2) l'inclusion des effets thermiques; et

(3) l'inclusion d'une capacité améliorée de raffinement des mailles (entre autres).

Yee, E., Lien, F.S. and Ji, H. (2007). Technical Description of Urban Microscale Modeling System: Component 1 of CRTI Project 02-0093RD. (DRDC Suffield TR 2007-067). Defence R&D Canada – Suffield.

Table of contents

Abstract	i
Résumé.....	ii
Executive summary	iii
Sommaire	iv
Table of contents	vi
List of figures.....	vii
Introduction	1
Background.....	1
Overview of the urban microscale modeling system	3
Technical description of modules	4
Grid generator: urbanGRID	4
Flow solver: urbanSTREAM	7
Urban dispersion: urbanEU and urbanAEU	12
Numerical implementation	14
Finite-volume discretization.....	14
Pressure-correction algorithm	17
Boundary condition implementation.....	21
Application to real urban environment	23
Joint Urban 2003	24
Grid generation for Oklahoma City	24
Flow field.....	25
Urban dispersion	27
Conclusions.....	28
References	30

List of Figures

Figure 1. Relationship between various components of CRTI Project 02-0093RD	32
Figure 2. Various modules of Component 1	33
Figure 3. Illustration of the ray-casting approach	34
Figure 4. Determination of whether two line segments intersect each other	35
Figure 5. Finite volume and storage arrangement	36
Figure 6. Computational domain used for simulation of flow in Oklahoma City	37
Figure 7. Computational grid generated by urbanGRID for Oklahoma City	38
Figure 8. Satellite photograph of downtown Oklahoma City	39
Figure 9. Comparison of mean wind speed	40
Figure 10. Detectors (squares) were positioned in the CBD sampling grid	41
Figure 11. Mean plume concentration isopleths	42
Figure 12. Influence function isopleths	43
Figure 13. Comparison of predicted mean concentrations	44
Figure 14. Comparison of predicted mean concentrations	45
Figure 15. Comparison of predicted mean concentrations	46

This page intentionally left blank.

Introduction

Background

The environmental and toxicological impact of the downwind transport and diffusion of contaminants released into the atmosphere has become increasingly important in recent years. Considerable interest has been focused on the prediction of mean concentration levels downwind of contaminant sources in the turbulent atmospheric boundary layer. Consequently, atmospheric transport and diffusion models have played an important role in emergency response systems to toxic releases and have been used in calculating the transport, diffusion, and deposition of toxic chemical, biological, or radiological materials released (either accidentally or deliberately) into the turbulent atmospheric boundary layer over relatively smooth and horizontally homogeneous surfaces. For example, military and civilian (government and commercial) emergency response models commonly use standard Gaussian plume or puff models which employ semi-empirical relationships for plume or puff growth with the mean wind and turbulence field obtained either from similarity theory or from the use of simple diagnostic wind fields constructed from interpolation and/or extrapolation of sparse observational data. The advantages of these approaches for wind flow specification are their simplicity, general applicability in simple atmospheric conditions, and most importantly, their limited computational requirements. While this approach is useful for a landscape that is relatively flat and unobstructed, it is wholly inadequate for surface-atmosphere interactions over "complex" surfaces (viz., most of the real world) such as cities and other built-up areas.

It needs to be emphasized that as the fraction of the World's population that live in cities continues to grow, it is becoming increasingly important to address the urgent problem of modeling of the dispersion of toxic releases in the urban environment, characterized by extremely diverse length and time scales and complex geometries and interfaces. Indeed, a typical urban canopy consists of a large collection of buildings and other obstacles (e.g., cars lining a street, treed areas in city green spaces, etc.) that are aggregated into complex structures. When this rough surface interacts with the atmospheric flow within and above it, the disturbed flow field can become extremely complex (e.g., curved mean streamlines, large velocity gradients, sharp velocity discontinuities, flow separations and reattachments, cavity regions, recirculation zones, and strongly inhomogeneous turbulence). Understanding the complex flow of the wind through and above the urban environment and the dispersion of contaminants released into that flow is both necessary and important. In view of this, we require physically-based urban wind models that can provide the needed spatial pattern of urban wind statistics required to "drive" modeling of dispersion of contaminants within the street canyons of an urban environment (where it is venting of these street canyons that is important for determination of the contaminant concentrations).

This identified capability gap was the motivation for the development of an advanced emergency response system for chemical, biological, radiological and nuclear (CBRN) hazard prediction and assessment for the urban environment sponsored by Chemical, Biological, Radiological and Nuclear Research and Technology Initiative (CRTI) under Project 02-0093RD. The principal objective of this project was to develop an advanced, fully validated, state-of-the-science modeling system for the prediction of urban flow (i.e., turbulent flow through cities) and the concomitant problem of the dispersion of CBRN agents re-

leased into these complex flows. This system will allow the dispersion of CBRN materials to be modeled over a vast range of length scales at the appropriate resolution for each scale: namely, in the near field (up to about 2 km) where dispersion is governed by the micro-scale regime of the planetary boundary layer; to the intermediate field between about 2 and 20 km where dispersion is governed by the local or meso- γ scale; through the far field covering the range from about 20-200 km (meso- β scale) and from about 200-2000 km (meso- α scale) which correspond to dispersion at the regional scale; and, finally out to the very far field encompassing scales greater than about 2000 km corresponding to dispersion on the large (synoptic and global) scales. The development of this proposed high-fidelity, multi-scale and multi-physics modeling system will provide a real-time modeling and simulation tool for prediction of injuries, casualties, and contamination and for making relevant decisions (based on the strongest technical and scientific foundations) required in the support of Canada's more broadly based efforts at advancing counter-terrorism planning and operational capabilities.

The multi-scale modeling system for emergency response consists of five major components shown in the schematic diagram of Figure 1. These five components can be described briefly as follows. Component 1 involves the development of models to predict the mean flow and turbulence in the urban complex at the microscale (from the building and street scale up to a length scale of about 2 km). Two kinds of models have been developed for this purpose: namely, high-resolution building-aware models for urban flow where buildings are explicitly resolved; and, virtual building models for urban flow where groups of buildings are represented simply in terms of a distributed drag force.

Component 2 involves the inclusion of the effects of urban terrain on the subgrid scales of a mesoscale meteorological model (Global Environmental Multi-scale Local Area Model, or GEM LAM) through an urban parameterization. This parameterization is required to account properly for the area-averaged effects of form drag, increased turbulence production, heating and surface energy budget modification due to the presence of buildings/obstacles and urban land use within the urban environment. Component 3 involves coupling the urban microscale flow models developed in Component 1 with the urbanized mesoscale model developed in Component 2. The interface between the urban microscale flow models and the urbanized GEM LAM model is demanding in that the information transfer between the two models must honor physical conservation laws, mutually satisfy mathematical boundary conditions, and preserve numerical accuracy, even though the corresponding meshes might differ in structure, resolution, and discretization methodology.

Component 4 involves using the mean flow and turbulence predicted by the multi-scale flow model developed in Component 3 to "drive" a Lagrangian Stochastic (LS) model for the prediction of urban dispersion of CBRN agents. The application of LS models to atmospheric dispersion in general (and, urban dispersion in particular) is recommended because LS models (1) are (in principle) the most flexible and the most easily able to incorporate all the known statistical details on the complex urban flow and (2) are physically transparent, and easily adapted to handle particulates, biological or radioactive decay, dry and wet deposition, and other relevant source and sink mechanisms. Finally, Component 5 involves the validation of the multi-scale modeling system for both the urban flow and dispersion components.

A series of reports and user's guides describe the various model components of CRTI Project

02-0093RD. The primary objective of this report is to describe the present status (and, more specifically, the technical formulation) of the ongoing model development conducted under Component 1 of the project. In addition, the predictive capabilities of the urban microscale flow and dispersion models developed in Component 1 and applied in stand-alone mode are demonstrated by presenting results from a case study involving the comparison of model predictions with experimental data obtained from a comprehensive full-scale urban field experiment conducted in Oklahoma City, Oklahoma in July 2003 (Joint Urban 2003, or JU2003 field experiment).

Overview of the urban microscale modeling system

The urban modeling system developed for Component 1 of CRTI Project 02-0093RD includes five main modules: urbanGRID, urbanSTREAM, urbanEU, urbanAEU, and urbanPOST. These modules and how they interface with each other and with other project components are shown in Figure 2.

In the simplest terms, urbanGRID imports building information encoded in Environmental Systems Research Institute (ESRI) Shapefiles and uses this data to generate a structured grid over a user selected computational domain in a given cityscape. Furthermore, urbanGRID imports three-dimensional meteorological fields (e.g., mean wind, turbulence kinetic energy, etc.) provided by urban GEM LAM and uses this information to provide inflow boundary conditions for the urban microscale flow model.

The structured grid and inflow boundary conditions provided by urbanGRID are used as input by urbanSTREAM which is a computational fluid dynamics (CFD) model for the numerical simulation of the flows around and within the complex geometries of buildings in the cityscape. The flow solver urbanSTREAM provides the high-resolution wind and turbulence fields used by the two Eulerian grid dispersion models urbanEU (source-oriented) and urbanAEU (receptor-oriented) to simulate the dispersion of contaminants in the urban domain. These two urban dispersion models are based on the numerical solution of K -theory advection-diffusion equation or its adjoint. Finally, urbanPOST is used to process the primary output files from urbanSTREAM to provide an appropriate specification of wind statistics required as input by either the two Eulerian urban dispersion models urbanEU and urbanAEU or, alternatively, by the urban Lagrangian Stochastic (LS) particle model urbanLS (forward dispersion model) or urbanbLS (backward dispersion model) developed under Component 4 of CRTI Project 02-0093RD.

The memory management scheme used in urbanSTREAM, urbanEU, and urbanAEU is full dynamic array allocation which allows the maximum array dimensions in these models to be easily adjusted to match the requirements of a particular problem. The size of the grid for a specific application is determined in urbanGRID which provides an external parameter file that specifies the required array sizes for all the major arrays in urbanSTREAM. The latter model then dynamically allocates only the amount of memory required for the specific problem.

Technical description of modules

Grid generator: urbanGRID

urbanGRID is a program that is concerned with the automatic generation of structured grids (or meshes) in the computational domain for numerical solutions involving the complex geometry of buildings and other obstacles in the urban environment (real cityscape). This program provides a predetermined mesh which fills the entire computational domain, and serves as the input data for spatial discretization required to “drive” the flow solver program urbanSTREAM. The mesh determines the location in the domain at which the flow quantities will be evaluated as well as where boundary conditions need to be applied at all the walls and roofs of arbitrary-shaped buildings (and other solid surfaces) in the domain.

The geometric information on shapes and locations of buildings in the computational domain (corresponding to a region of a real city) is assumed to be available in form of ESRI Shapefiles [1]. An ESRI Shapefile is a digital vector storage format that stores non-topological information and spatial features in a data set, with the geometry for each feature comprising a set of vector coordinates and associated attribute information. A Shapefile is actually a set of files. Three individual files are mandatory and these store the core data, although in general a Shapefile may also include up to eight further optional individual files. urbanGRID only requires Shapefile information stored in the three mandatory files. These three individual files have the following file extensions in their name: (1) *.shp is the main file and is a direct-access, variable record-length file whose records store the feature geometry (for our current application, the key features are area features corresponding to building “footprints” encoded as closed-loop double-digitized polygons); (2) *.shx is the file that stores the index of the feature geometry and contains the offset of the main file record from the beginning of the main file; and, (3) *.dbf is a file in the form of a dBASE table that contains feature attributes (e.g., height of buildings) with one record per feature, there being a one-to-one correspondence between the geometry and attributes based on record number.

The computational domain where the flow field will be calculated is specified by the user who provides the x and y coordinates (easting and northing coordinates, respectively) of the southwest (x_{SW}^{outer} , y_{SW}^{outer}) and northeast (x_{NE}^{outer} , y_{NE}^{outer}) corners of the domain in the Universal Transverse Mercator (UTM) coordinate system. Additionally, the user provides the easting and northing coordinates of the southwest (x_{SW}^{inner} , y_{SW}^{inner}) and northeast (x_{NE}^{inner} , y_{NE}^{inner}) corners for an inner domain which lies strictly inside the computational domain where buildings are explicitly resolved (building-aware region) in the sense that appropriate boundary conditions are imposed on all the building surfaces (e.g., wall, roofs). For the region that lies outside the inner domain but inside the computational domain, the buildings are treated as virtual in the sense that the effects of these unresolved buildings on the flow are represented simply as a distributed mean-momentum sink in the mean momentum equations (which is described later in this report). urbanGRID uses the Shapefile C Library Version 1.2 (Shapelib) [2] for reading ESRI Shapefiles, and of greatest interest here, are the vector coordinates of all the vertices (ordered in a counter-clockwise direction) that define the footprints of the buildings (which are represented in UTM coordinates) and the attribute corresponding to the heights of the buildings in the inner domain. Finally, the height z_d of

Once the computational domain has been defined, a structured Cartesian mesh is generated over the domain. The implicit grid structure alleviates the need to store the mesh connectivity, and permits the use of rapid iterative solution algorithms for the computation of the flow, which makes use of sparse matrix solvers. urbanGRID generates a Cartesian mesh over the computational domain by defining an arrangement of discrete grid points that define the cell faces (grid lines). In any given coordinate direction, the spacing of the grid points starting from a solid surface (e.g., ground surface, wall or roof of building, etc.) is stretched as one moves away from the surface along the coordinate direction. The stretching function used in urbanGRID has the form

where L_i is the length of the domain in the i -th coordinate direction, N_i is the number of grid points in the i -th coordinate direction, $x_i[j]$ is the j -th grid point coordinate in the i -th coordinate direction for a uniform grid spacing, and $x_{s,i}[j]$ is the corresponding j -th grid point coordinate in the i -th direction for the stretched grid. In Equation (1), $\alpha \in \{0, \frac{1}{2}, 1\}$ and $\beta \in (1, \infty)$ are parameters of the stretching function that are used to determine, respectively, the direction (positive, negative, or in both directions) of stretching along the coordinate axis and the magnitude of the stretching. More specifically, if $\alpha = 0$ the spacing between the grid points is stretched along the positive direction of the x_i -axis, if $\alpha = 1$ the stretching is applied along the negative direction of the x_i -axis, and if $\alpha = \frac{1}{2}$ the stretching is along both the negative and positive directions of the x_i -axis. Finally, the stretching of the spacing between grid points along a coordinate axis increases as $\beta \rightarrow 1^+$, whereas $\beta \rightarrow \infty$ results in a uniform spacing between grid points.

In the inner region of the computational domain, the buildings are explicitly resolved and it becomes imperative to define an appropriate data structure to encode information about whether a control volume (grid cell) is a fluid cell (which lies mostly or completely within the fluid region) or an obstacle cell (which lies mostly or completely inside a building), and if a fluid cell whether any face of this cell abuts against a wall or roof of a building (the latter information being required for the implementation of the wall function boundary condition in urbanSTREAM). To this purpose, urbanGRID uses an 8-bit integer **FLAG** array to encode this information as follows:

If bit number 7 (C_0 bit) of the FLAG array is set for a cell with indices (i, j, k) (viz., $\text{FLAG}(i, j, k) = \text{C_0} = 64$), then this cell is an obstacle cell; otherwise, it is a fluid cell. Bit number 8 (C_D bit) of the FLAG array determines whether the cell lies in the region where buildings are considered to be virtual and, hence, represented as a distributed momentum drag force in the mean momentum equation. More specifically, if bit 8 is switched on in the FLAG array for cell (i, j, k) then this cell lies within the “virtual building” region of the computational domain. The remaining lower-order bits of the FLAG array determine

whether a fluid cell is also a boundary cell in the sense that one or more faces of this cell borders an obstacle cell. For example, a fluid cell for which the lowest bit (or, C_E bit) of the FLAG array is ON signifies that the east face of the corresponding fluid cell abuts against a building surface. Similarly, the second (C_W), third (C_N), fourth (C_S), fifth (C_T), and sixth (C_B) bits of the FLAG array if switched ON imply that the west, north, south, top, or bottom faces of the associated fluid cell borders on a building surface.

Because each building extracted from an ESRI Shapefile has a constant height attribute, it is computationally more efficient to consider the intersection of the projection of the cell in the horizontal x - y plane with the building footprint (represented by a closed-loop polygon in the Shapefile) in order to determine whether a particular grid cell is a fluid cell or an obstacle cell. To this end, a bounding box (or, smallest rectangle that completely surrounds the building footprint and has sides that are parallel to the x -axis and y -axis) is constructed for each building within the inner (or, building-aware) region. Clearly, only grid cells that intersect any of these bounding boxes in the inner region can possibly be classified as obstacle cells (with the appropriate bit in the associated FLAG array set); otherwise, the grid cell must necessarily be classified as a fluid cell.

For the grid cells that intersect one of the bounding boxes in the inner region, the determination of whether these cells are obstacle or fluid cells depends on whether the centroid of the cell lies inside or outside the building, respectively. A ray-casting approach is used to ascertain this condition. As shown in Figure 3, the ray-casting approach for determination of whether a grid cell should be classified as a fluid cell or obstacle cell involves casting a ray \mathbf{r} from the cell centroid \mathbf{c} and simply counting the number of intersections of \mathbf{r} with the various faces of the building enclosed by the bounding box that the grid cell overlaps. If the grid cell centroid lies inside a building (labeled B in Figure 3), the number of intersections of \mathbf{r} with the building faces must be odd. Because the building footprint is encoded as a list of vector coordinates of vertices forming a number of line segments that constitute a closed polygon, we need to determine if there is an intersection of ray \mathbf{r} with each of these line segments and then count the total number of intersections.

The determination of whether two line segments intersect is based on the computation of a signed area. To this purpose, let us focus on whether line segment \overline{ab} intersects line segment \overline{cd} as depicted in Figure 4. To ascertain this, we calculate the signed areas for the following four triangles: $\Delta(acd)$, $\Delta(bcd)$, $\Delta(acb)$ and $\Delta(adb)$. The signed area for a triangle $\Delta(abc)$ whose three vertices are a , b and c (ordered in either a clockwise or counter-clockwise direction) is given by

$$A_{abc} = \det \begin{pmatrix} a_x & a_y & 1 \\ b_x & b_y & 1 \\ c_x & c_y & 1 \end{pmatrix}, \quad (2)$$

where $a = (a_x, a_y)$, $b = (b_x, b_y)$ and $c = (c_x, c_y)$. With reference to Figure 4, the two line segments \overline{ab} and \overline{cd} intersect each other if and only if the following two conditions are verified:

$$\begin{aligned} A_{acd} \times A_{bcd} &< 0, \\ A_{acb} \times A_{adb} &< 0. \end{aligned} \quad (3)$$

While the test for intersection of two line segments provided by Equation (3) is straightforward, its implementation on the necessarily finite precision of the hardware on a digital

computer is not. Problems can arise when a zero-area triangle corresponding to the case when the vertices of a triangle are exactly collinear. Given the finite precision of a digital computer, distinguishing between the case of a zero-area triangle occurring because of round-off error and precision problems or because of an exact collinearity is difficult and needs to be handled carefully. To deal with this possibility, urbanGRID uses an adaptive exact arithmetic procedure developed by Schewchuk [3] in its computation of signed areas. The procedure used in urbanGRID for this is as follows. We first calculate the signed area given by Equation (2) using floating point arithmetic, and then estimate the maximum possible value for the round-off error using the error bound derived in [3]. If this error is larger than the computed signed area, then the area is re-calculated using adaptive precision floating point arithmetic. If this result is identically zero too, then we resolve the degeneracy in the signed area computation by using a “tie-breaking” algorithm based on a virtual perturbation approach advocated by Edelsbrunner and Muncke [4]. The basic idea underpinning this approach is to resolve “ties” in the vector coordinates of the triangular vertices that result in an “exact” zero signed area by breaking this degeneracy through the introduction of a unique and ordered perturbation of the vertices. This results in a non-degenerate signed area. Since the perturbation is virtual, no geometric data is modified. It is noted that this refinement is merely a technicality needed to resolve possible finite precision collinearity of vertices of a triangle. The virtual perturbation of the vertices never affects the actual coordinates of these vertices (which are always held to finite precision), but nevertheless enables an unambiguous calculation of the signed area.

The distribution of flow variables needs to be specified (viz., Dirichlet boundary conditions need to be defined) at the inflow boundary planes for the computational domain used for flow calculation in urbanSTREAM. To this purpose, urbanGRID interpolates the gridded mean velocity and turbulence fields provided by urban GEM LAM (a prognostic mesoscale model with an urban parameterization developed by Environment Canada for CRTI Project 02-0093RD). The gridded mean velocity and turbulence kinetic energy fields provided by urban GEM LAM in a large domain that includes the computational domain defined in urbanGRID are linearly interpolated to the grid nodes in the inflow boundary planes for urbanSTREAM. This corresponds to a one-way coupling between the mesoscale flow model urban GEM LAM and the microscale (building-aware) flow model urbanSTREAM.

Flow solver: urbanSTREAM

The prediction of the complex flow (mean wind and turbulence quantities) through and above an urban canopy consisting of groups of buildings in various configurations that are representative of a real cityscape is based on the Reynolds-averaged Navier-Stokes (RANS) equations whereby the turbulent flow is considered as consisting of two components: a fluctuating part and a mean or average part. The Reynolds-averaged continuity and momentum equations for an incompressible adiabatic (i.e., not buoyancy-affected) fluid are a system of partial differential equations governing mass and momentum conservation and can be expressed in Cartesian coordinates as follows:

Continuity

$$\frac{\partial \bar{u}_i}{\partial x_i} = 0, \quad (4)$$

Momentum

$$\frac{\partial \bar{u}_i}{\partial t} + \frac{\partial \bar{u}_j \bar{u}_i}{\partial x_j} = -\frac{\partial \bar{p}}{\partial x_i} + \nu \frac{\partial^2 \bar{u}_i}{\partial x_j^2} - \frac{\partial}{\partial x_j} (\overline{u'_i u'_j}) - 2\epsilon_{ijk} \Omega_j \bar{u}_k, \quad (5)$$

where the Reynolds averaging of a quantity is denoted by drawing a bar over the quantity. Summation is implied by repeated indices. Here, \bar{u}_i and u'_i are the mean and fluctuating velocities in the x_i -direction, respectively, with $i = 1, 2$, or 3 representing the west-east x , south-north y , or vertical z directions; $x_i = (x, y, z) \equiv \mathbf{x}$; t is time; $u_i = (u, v, w)$; $\bar{u}_i = (\bar{u}, \bar{v}, \bar{w})$; ν is the kinematic viscosity and \bar{p} is the kinematic mean pressure (with p' used to denote pressure fluctuations). The last term on the right-hand-side (RHS) of Equation (5) is the Coriolis acceleration term (caused by the Coriolis force) where Ω_j is the Earth's rotation vector and ϵ_{ijk} is the permutation symbol (which has the value zero if any pair of subscripts is identical, and is $(-1)^q$ otherwise where q is the number of subscript transpositions required to bring (ijk) to the natural order (123)). Rotation is defined by the right-hand rule where positive is clockwise when looking in the direction of Ω_j . Note that the Cartesian coordinate system fixed on the Earth's surface can have any orientation with respect to Ω_j .

Reynolds-averaging the Navier-Stokes equation gives rise to the so-called kinematic Reynolds stresses which are defined as the tensor $\overline{u'_i u'_j}$. The Reynolds stresses depend on the velocity fluctuations u'_i , and introduce new unknown quantities in the RANS equations, and therefore these equations no longer constitute a closed system. In order to close the system of equations, we need further equations describing the relationship between $\overline{u'_i u'_j}$ and the quantities \bar{u}_i and \bar{p} that we seek to determine. This is known as the closure problem in turbulence modeling. One of the simplest turbulence models for $\overline{u'_i u'_j}$ involves approximating the Reynolds stress components by analogy with a Newtonian type of linear constitutive relationship between the turbulence stress and the mean strain-rate tensor. This model uses the Boussinesq eddy-viscosity approximation (which is perhaps the simplest coordinate invariant relationship between stresses and strains) and is given by

$$\overline{u'_i u'_j} = \frac{2}{3} k \delta_{ij} - \nu_t \left(\frac{\partial \bar{u}_i}{\partial x_j} + \frac{\partial \bar{u}_j}{\partial x_i} \right), \quad (6)$$

where ν_t is the kinematic eddy viscosity, $k \equiv \frac{1}{2} \overline{u'_i u'_i}$ is the turbulence kinetic energy (TKE), and δ_{ij} is the Kronecker delta function. It is interesting to note that with the adoption of the Boussinesq eddy-viscosity approximation, the RANS equations have the same form as the Navier-Stokes equations except that the kinematic molecular viscosity ν is replaced by an effective kinematic viscosity $\nu_{\text{eff}} = (\nu + \nu_t)$ and provided the mean pressure is interpreted to be a modified mean pressure¹.

With the Boussinesq eddy-viscosity model (EVM) for the Reynolds stresses, the task of turbulence closure reduces to the determination of the eddy viscosity. Dimensional analysis dictates that the eddy viscosity ν_t be determined by the product of a turbulence velocity scale u_0 and a turbulence length scale l_0 , so

$$\nu_t = u_0 l_0,$$

¹ When Equation (6) is inserted into Equation (5), the term $\frac{2}{3} k \delta_{ij}$ in the Boussinesq approximation for the Reynolds stresses is usually incorporated with the pressure \bar{p} to define a modified pressure $\bar{p} + \frac{2}{3} k$ (so, $\bar{p} \rightarrow \bar{p} + \frac{2}{3} k \equiv \bar{p}^{\text{mod}}$ in the RANS equations).

where u_0 and l_0 can vary significantly in space and time for a given turbulent flow (and, in particular, for an urban flow). In the most common approach, the turbulence velocity and length scales are based on the turbulence kinetic energy k and its dissipation rate ϵ (i.e., rate at which TKE is converted into thermal internal energy), with the turbulence velocity and length scales chosen to be

$$u_0 = C_\mu^{1/4} k^{1/2}, \quad l_0 = \frac{u_0^3}{\epsilon}. \quad (7a)$$

Hence, in this so-called k - ϵ modeling framework at high-Reynolds (high-Re) numbers, the eddy viscosity is given by (on combining turbulence velocity and length scales)

$$\nu_t = C_\mu \frac{k^2}{\epsilon}, \quad (7b)$$

where C_μ is a closure constant.

The modeled transport equation for the turbulence kinetic energy k is

$$\frac{\partial k}{\partial t} + \frac{\partial \bar{u}_j k}{\partial x_j} = \frac{\partial}{\partial x_j} \left[\left(\nu + \frac{\nu_t}{\sigma_k} \right) \frac{\partial k}{\partial x_j} \right] + P_k - \epsilon, \quad (8)$$

where P_k is the production of k defined as

$$P_k \equiv -\overline{u'_i u'_j} \frac{\partial \bar{u}_i}{\partial x_j}. \quad (9)$$

The terms in the modeled TKE transport equation [Equation (8)] are from left to right: local rate of change of k , transport of k by mean advection, transport of k by viscous and turbulent diffusion, rate of production of k , and rate of destruction of k . Within the framework of a two-equation turbulence closure scheme, the turbulent diffusion term in the exact transport equation for TKE is modeled using a gradient diffusion hypothesis as

$$\bar{D}_j^t \equiv - \left[\frac{1}{2} \overline{u'_i u'_i u'_j} + \overline{p' u'_i} \delta_{ij} \right] = \frac{\nu_t}{\sigma_k} \frac{\partial k}{\partial x_j}, \quad (10)$$

where σ_k is a constant that functions like an effective Schmidt number for the turbulent diffusion of k . Note that, with this model, both the turbulent and molecular diffusion terms can be combined into a gradient transport model with effective viscosity $(\nu + \nu_t/\sigma_k)$. This resulting simple form of the modeled transport equation for k is the obvious appeal of this formulation.

An exact transport equation for ϵ can be written, but this equation is not useful owing to the fact that most of the terms in the equation are not in closed form. In its most usual form, the modeled equation for the TKE dissipation rate ϵ is

$$\frac{\partial \epsilon}{\partial t} + \frac{\partial \bar{u}_j \epsilon}{\partial x_j} = \frac{\partial}{\partial x_j} \left[\left(\nu + \frac{\nu_t}{\sigma_\epsilon} \right) \frac{\partial \epsilon}{\partial x_j} \right] + \frac{\epsilon}{k} (C_{\epsilon 1} P_k - C_{\epsilon 2} \epsilon), \quad (11)$$

where $C_{\epsilon 1}$, $C_{\epsilon 2}$ and σ_ϵ are closure constants to be determined. In Equation (11), the turbulent diffusion of dissipation (which has been grouped with the molecular diffusion term) is given by

$$\bar{D}_\epsilon^t = \frac{\partial}{\partial x_j} \left[\frac{\nu_t}{\sigma_\epsilon} \frac{\partial \epsilon}{\partial x_j} \right], \quad (12)$$

where σ_ϵ is a constant that acts like an effective Schmidt number for the turbulent diffusion of TKE dissipation. In Equation (11), the term on the RHS that involves $C_{\epsilon 1}$ is the production of dissipation term, whereas the term involving $C_{\epsilon 2}$ is the destruction of dissipation term. The factor ϵ/k in the production and destruction terms makes these terms dimensionally correct in the transport equation for ϵ .

Within the Boussinesq type of eddy-viscosity approximation, the Reynolds stresses appearing in the production P_k [cf. Equation (9)] are modeled in accordance with Equation (6) resulting in the following modeled form for P_k :

$$P_k = \nu_t \left(\frac{\partial \bar{u}_i}{\partial x_j} + \frac{\partial \bar{u}_j}{\partial x_i} \right) \frac{\partial \bar{u}_i}{\partial x_j} = C_\mu \epsilon |\bar{S}|^2, \quad (13)$$

where

$$|\bar{S}| = \frac{k}{\epsilon} (2\bar{S}_{ij}\bar{S}_{ij})^{1/2}, \quad \bar{S}_{ij} \equiv \frac{1}{2} \left(\frac{\partial \bar{u}_i}{\partial x_j} + \frac{\partial \bar{u}_j}{\partial x_i} \right). \quad (14)$$

Here, \bar{S}_{ij} is the mean rate-of-strain tensor (or, equivalently, the symmetric part of the mean velocity gradient tensor).

Together, the transport equations for k and ϵ contain five closure constants (C_μ , σ_k , σ_ϵ , $C_{\epsilon 1}$, and $C_{\epsilon 2}$) which must be determined before the equations can be solved. Two different high-Re number k - ϵ models are considered here. The first is the standard k - ϵ model and following the recommendation of Launder and Spalding [5], the closure coefficients for this turbulence model are

$$C_\mu = 0.09, \quad \sigma_k = 1, \quad \sigma_\epsilon = 1.3, \quad C_{\epsilon 1} = 1.44, \quad C_{\epsilon 2} = 1.92. \quad (15)$$

Here, $C_{\epsilon 2}$ is determined from the experiment on the decay of isotropic turbulence, and $C_{\epsilon 1}$ is determined experimentally based on the local equilibrium wall shear flow. The value of σ_ϵ is chosen to ensure the correct log-law behaviour in boundary-layer flows. The second k - ϵ model implemented is the limited-length-scale k - ϵ model proposed by Apsley and Castro [6]. In this modified k - ϵ model the length-scale determining equation (i.e., ϵ -transport equation) is modified in order to acknowledge the upper bounds on the turbulence length scale imposed by the finite depth of the atmospheric boundary layer. The modification is both simple and elegant; namely, the coefficient $C_{\epsilon 1}$ in the production of dissipation term is replaced by

$$C_{\epsilon 1} \rightarrow C_{\epsilon 1} + (C_{\epsilon 2} - C_{\epsilon 1}) \frac{l_0}{l_{0,\max}}, \quad (16)$$

where $l_{0,\max} = h/3$ is the maximum turbulence length scale imposed by the depth h of the atmospheric boundary layer [and l_0 is defined in Equation (7a)]. It is noted that with the exception of $l_{0,\max}$, the modification introduces no new closure constants into the model (viz., the closure constants C_μ , σ_k , σ_ϵ , $C_{\epsilon 1}$, and $C_{\epsilon 2}$ assume exactly the same values as in the standard k - ϵ model).

A closed-form solution for the k - ϵ model can be obtained for the neutral wall shear layer. The solution gives

$$\bar{u} = \frac{u_*}{k_v} \log z + B, \quad k = \frac{u_*^2}{\sqrt{C_\mu}}, \quad \epsilon = \frac{u_*^3}{k_v z}, \quad (17)$$

where $u_* \equiv (-\overline{u'w'})^{1/2}$ is the friction velocity and B is a constant of integration. For this analytical solution, we find an implied value for the von Kármán constant, k_v , of

$$k_v^2 = \sqrt{C_\mu}(C_{\epsilon 2} - C_{\epsilon 1})\sigma_\epsilon. \quad (18)$$

Using the closure coefficient values for the k - ϵ model, k_v assumes a value of 0.43. The experimental values for k_v are primarily in the range 0.41 ± 0.2 , so the implied value of k_v in the k - ϵ model is consistent with these measurements. The stress-intensity ratio, u_*^2/k , is predicted to be 0.3 (using $C_\mu = 0.09$) which agrees well with experimental measurements of this quantity in many shear flows [7].

The technical details of urbanSTREAM used in the high-resolution computational fluid dynamics simulation of urban flow where all the buildings in the computational domain are explicitly resolved in the sense that appropriate boundary conditions are imposed at all the building surfaces (e.g., walls, roofs), have been described. However, the computational demands of such an approach are high and, as a consequence, sufficiently prohibitive as to preclude the simulation of flow through and above all buildings over a relatively large computational domain in a typical city environment.

In lieu of imposing correct boundary conditions on the true (but usually complex, three-dimensional) geometry of the building surfaces and fully resolving the detailed intricate flow around every individual building in a computational domain, it is convenient to consider the prediction of statistics of the mean wind and turbulence in an urban canopy that are obtained by averaging horizontally the flow properties over an area that is larger than the spacings between the individual roughness elements comprising the urban canopy, but less than the length scale over which the roughness element density changes. Towards this objective, we consider the use of a virtual building concept in urbanSTREAM whereby groups of buildings are unresolved and the aggregate of these individual buildings is treated simply as a porous medium. Here, the effects of the unresolved buildings (or, virtual buildings) on the flow are represented through a distributed mean-momentum sink in the mean momentum equation. Furthermore, the additional source/sink terms in the supporting transport equations for k and ϵ are included in order to model the effects of the virtual buildings on the turbulence.

The foundations of a systematic mathematical formulation for the derivation of the governing equations for flow through an urban canopy where the individual buildings are unresolved (virtual buildings) and the aggregate of various groups of buildings (and other obstacles) is treated simply as a porous medium is described in Lien, Yee and Wilson [8]. The representation of groups of buildings as a porous medium requires an additional modeling effort. The transport equation for the mean momentum is modified with the inclusion of a mean drag force $\bar{f}_{d,i}$ due to the effects of the virtual buildings on the flow, so

$$\frac{\partial \bar{u}_i}{\partial t} + \frac{\partial \bar{u}_j \bar{u}_i}{\partial x_j} = -\frac{\partial \bar{p}}{\partial x_i} + \nu \frac{\partial^2 \bar{u}_i}{\partial x_j^2} - \frac{\partial}{\partial x_j}(\overline{u'_i u'_j}) - 2\epsilon_{ijk}\Omega_j \bar{u}_k + \bar{f}_{d,i}, \quad (19)$$

where $\bar{f}_{d,i}$ is parameterized as follows:

$$\bar{f}_{d,i} = -\hat{C}_D \hat{A} \left(Q \bar{u}_i + \frac{\bar{u}_j}{Q} \overline{u'_i u'_j} + \frac{\bar{u}_i k}{Q} \right), \quad (20)$$

where \hat{C}_D is the drag coefficient, \hat{A} is the frontal area density (frontal area of buildings exposed to the wind per unit volume), and $Q \equiv (\bar{u}_i \bar{u}_i)^{1/2}$ is the magnitude of the (spatially-averaged) time-mean wind speed. Utilizing the eddy viscosity model for turbulent stresses of Equation (6) in Equation (20) yields the following final form for the mean drag force imposed by the virtual buildings on the flow:

$$\bar{f}_{d,i} = -\hat{C}_D \hat{A} \left[\left(Q + \frac{5}{3} \frac{k}{Q} \right) \bar{u}_i - \nu_t \left(\frac{\partial \bar{u}_i}{\partial x_j} + \frac{\partial \bar{u}_j}{\partial x_i} \right) \frac{\bar{u}_j}{Q} \right]. \quad (21)$$

Standard turbulence models need additional modifications when applied to urban flows where buildings are treated as virtual (and represented as a distributed mean-momentum sink). Additional modifications required in the transport equations for k and ϵ were derived in [8] and are simply summarized here. The k - and ϵ -equations require additional source/sink terms and now take the following form:

$$\frac{\partial k}{\partial t} + \frac{\partial \bar{u}_j k}{\partial x_j} = \frac{\partial}{\partial x_j} \left[\left(\nu + \frac{\nu_t}{\sigma_k} \right) \frac{\partial k}{\partial x_j} \right] + (P_k + F) - \epsilon, \quad (22)$$

and

$$\frac{\partial \epsilon}{\partial t} + \frac{\partial \bar{u}_j \epsilon}{\partial x_j} = \frac{\partial}{\partial x_j} \left[\left(\nu + \frac{\nu_t}{\sigma_\epsilon} \right) \frac{\partial \epsilon}{\partial x_j} \right] + \frac{\epsilon}{k} (C_{\epsilon 1} (P_k + F) - C_{\epsilon 2} \epsilon). \quad (23)$$

The term F in Equation (22) can be interpreted as an additional physical mechanism for the production/dissipation of k , and as shown in [8] can be approximated as

$$F = -\hat{C}_D \hat{A} \left[2Qk + \frac{1}{Q} \left(\bar{u}_i \bar{u}_k \overline{u'_i u'_k} \right) + \frac{3}{2Q} \left(\bar{u}_k \overline{u'_i u'_i u'_k} \right) \right], \quad (24)$$

where the triple correlation term $\overline{u'_i u'_i u'_k}$ here is modelled, following Daly and Harlow [9], as

$$\overline{u'_i u'_i u'_k} = 2C_s \frac{k}{\epsilon} \left[\overline{u'_k u'_l} \frac{\partial k}{\partial x_l} + \overline{u'_i u'_l} \frac{\partial \overline{u'_i u'_k}}{\partial x_l} \right], \quad (25)$$

where the closure constant $C_s \approx 0.3$ is used in the present study. The double correlation (turbulent stress) $\overline{u'_i u'_j}$ in Equations (24) and (25) are modelled using the Boussinesq stress-strain relationship in Equation (6).

Urban dispersion: urbanEU and urbanAEU

Prediction of the wind field statistics using urbanSTREAM is in principle pre-requisite to or co-requisite with prediction of the simpler (but nevertheless complex) problem of scalar (contaminant) diffusion within the urban environment. In particular, the prediction of turbulent flow statistics through a built-up area is required to provide the input information needed to “drive” a physically-based model for urban dispersion. Within the context of Component 1 of CRTI Project 02-0093RD, two different (but complementary) models for urban dispersion from the Eulerian perspective have been developed, and will be described in this sub-section.

The first urban dispersion model, referred to as urbanEU, uses a source-oriented dispersion modeling technique. The model estimates dispersion about the flow within the urban canopy (viz., at the street and neighborhood scale) for passive scalars released into that flow. In consequence, the mean momentum equation is decoupled from the scalar transport equation with the velocity field independent of the scalar concentration field. More specifically, the additional transport equation required for the conservation of the scalar (the contaminant) has the following form:

$$\frac{\partial C}{\partial t} + \frac{\partial \bar{u}_j C}{\partial x_j} = \frac{\partial}{\partial x_j} \left[(K + K_t) \frac{\partial C}{\partial x_j} \right] + Q, \quad (26)$$

where C is the concentration of a contaminant (g m^{-3}), K is the molecular kinematic diffusivity of the contaminant in air ($\text{m}^2 \text{s}^{-1}$), K_t is the turbulent (or, eddy) kinematic diffusivity ($\text{m}^2 \text{s}^{-1}$), and Q is the source density distribution for the contaminant ($\text{g s}^{-1} \text{m}^{-3}$).

In Equation (26), a gradient diffusion model is used as perhaps the simplest closure model for the turbulent scalar fluxes, although this assumption has not been rigorously justified for urban dispersion. In particular, within this popular framework the turbulent scalar fluxes are modeled as

$$\overline{u'_j c'} = -K_t \frac{\partial C}{\partial x_j}, \quad (27)$$

and the turbulent diffusivity K_t is obtained from the turbulent viscosity ν_t (predicted by urbanSTREAM) in combination with a turbulent Schmidt number Sc_t in the following manner:

$$K_t = \frac{\nu_t}{Sc_t}. \quad (28)$$

In urbanEU, we adopt this concept using a constant turbulent Schmidt number Sc_t with a value of 0.63. This value for Sc_t was chosen with reference to Project Prairie Grass, a benchmark field experiment documenting turbulent dispersion from a continuous point source near the ground into the atmospheric surface layer, where it has subsequently been shown that an Eulerian dispersion model is in excellent conformance with these high-quality experimental measurements provided the turbulent Schmidt number has a value $Sc_t \approx 0.63$ (Wilson [10]).

In the source-oriented dispersion model implemented by urbanEU, the goal of the dispersion modeling is to calculate the mean concentration ‘seen’ by a detector at a given receptor location when provided the source distribution (source term) Q of the contaminant. In other words, in the source-oriented approach the advection-diffusion equation given by Equation (26) is solved forward in time for a given source distribution of contaminant $Q(\mathbf{x}, t)$ to obtain the mean concentration field $C(\mathbf{x}, t)$. Then, the concentration of contaminant ‘seen’ by a detector at a given receptor, denoted $\Phi(C)$, can be defined as the following integral of concentration $C(\mathbf{x}, t)$ filtered in space and time by the spatial-temporal filtering function $h(\mathbf{x}, t)$ corresponding to the response function of the detector:

$$\Phi(C) = \int C(\mathbf{x}, t) h(\mathbf{x}, t) d\mathbf{x} dt \equiv (C, h). \quad (29)$$

Therefore, this integral is simply a linear functional of C and expresses averaging of the concentration field over the spatial volume and averaging time imposed by the detector at

the receptor location. This linear functional of C is defined by the inner product (C, h) given in Equation (29), and allows one to calculate detector concentrations at any number of receptors located within the computational domain. However, for any new release scenario involving a different source distribution Q , the solution of Equation (26) needs to be calculated again in order to determine Φ .

Alternatively, when the detector concentration at a fixed receptor is of principal interest for a range of different emission scenarios, the alternative receptor-oriented dispersion modeling approach is useful. As a result, we have implemented a receptor-oriented dispersion model in urbanAEU, which solves the following adjoint advection-diffusion equation for the influence (or, adjunct) function C^* (m^{-3}):

$$-\frac{\partial C^*}{\partial t} - \frac{\partial \bar{u}_j C^*}{\partial x_j} = \frac{\partial}{\partial x_j} \left[(K + K_t) \frac{\partial C^*}{\partial x_j} \right] + h, \quad (30)$$

where h is the space-time filtering function of the detector at the fixed receptor location. It is important to note that Equation (30) is the adjoint of Equation (26) with C and C^* related to each other through the source function Q and detector (receptor) function h as follows:

$$\Phi(C) = \int C^*(\mathbf{x}, t) Q(\mathbf{x}, t) d\mathbf{x} dt \equiv (C^*, Q) = (C, h). \quad (31)$$

Equation (31) is a duality relation that relates C with C^* through Q and h and, in this sense, C and C^* can be interpreted as dual quantities. In the receptor-oriented approach, Equation (30) is solved backwards in time for a given receptor, and the concentration ‘seen’ by a detector at this receptor can now be calculated directly using Equation (31) once the source distribution Q has been specified. It should be noted that these computations can be repeated for any source distribution Q to obtain the concentration at the given receptor without having to re-solve Equation (30) for C^* . However, a new adjunct function C^* needs to be determined if the concentration is desired for a different receptor.

Numerical implementation

Finite-volume discretization

The coupled, nonlinear system of six partial differential equations which models unsteady, three-dimensional turbulent flow field in urbanSTREAM and the partial differential equation describing scalar transport in urbanEU and urbanAEU are solved using a finite-volume method. All these partial differential equations have the following generic form:

$$\frac{\partial \phi}{\partial t} + \frac{\partial \bar{u}_j \phi}{\partial x_j} = \frac{\partial}{\partial x_j} \left(\Gamma_\phi \frac{\partial \phi}{\partial x_j} \right) + S_\phi, \quad (32)$$

for a scalar ϕ (which can be identified with any of the mean Cartesian velocity components \bar{u}_i , turbulence kinetic energy k , viscous dissipation ϵ , mean concentration C , or influence function C^*); Γ_ϕ is the diffusivity and S_ϕ represents the source/sink term. If the current time level for ϕ is denoted by the superscript $n + 1$ and the time increment by Δt , a two- or three-level time discretization can be used to approximate the local rate of change of ϕ as follows:

$$\left(\frac{\partial \phi}{\partial t} \right)^{n+1} \approx \frac{1}{2\Delta t} (a_0 \phi^{n+1} + a_1 \phi^n + a_2 \phi^{n-1}), \quad (33)$$

where $a_0 = -a_1 = 2$, $a_2 = 0$ for first-order accuracy (using only two time levels) and $a_0 = 3$, $a_1 = -4$, $a_2 = 1$ for second-order accuracy. Both options are available in urbanSTREAM and urban(A)EU for approximating temporal derivatives. Finally, in the discretization to follow, it is assumed that the source/sink term S_ϕ , which may be a nonlinear function of ϕ , is linearized as follows:

$$S_\phi \approx S_P \phi + S_C, \quad (34)$$

where it is implicitly assumed that S_P is chosen to be unconditionally negative.

Integration of the transport equation governing the flow property ϕ in Equation (32) over the finite volume (or, control volume) shown in Figure 5, use of the time discretization of Equation (33) to approximate the local tendency term, and application of the divergence theorem results in a discretized transport equation for ϕ that expresses a balance of local flow property change, advective and diffusive fluxes of the flow property across the cell faces, and generation/destruction of ϕ embodied by the volume-integrated net source/sink term. The resulting full implicit time discrete version of Equation (32) takes the following form [on insertion of the linearization of S_ϕ given by Equation (34)]:

$$a_P \phi_P^{n+1} = \sum_{nb} a_{nb} \phi_{nb}^{n+1} + Q_C, \quad (35a)$$

where

$$Q_C = S_C \Delta\Omega - \frac{\Delta\Omega}{2\Delta t} [a_1 \phi^n + a_2 \phi^{n-1}] \quad (35b)$$

($\Delta\Omega$ is the volume of the cell with center node P); nb refers to the six neighbors of cell center P associated with nodes at the cell centers to the west (W), east (E), south (S), north (N), bottom (B), and top (T) of the center node P ; and, the six surfaces (faces) of the control volume centered at P will be denoted using lower-case letters corresponding to their direction (w , e , s , n , b and t) with respect to P (see Figure 5). The surface area of a cell face in direction κ relative to the cell center P will be denoted by A_κ ($\kappa \in \{w, e, s, n, b, t\}$).

The influence coefficients (not to be confused with the influence function C^*) a_{nb} ($nb \in \{W, E, S, N, B, T\}$) of the neighboring unknowns of the flow property ϕ take the following form, assuming that the diffusive fluxes have been approximated by central differences and the advective fluxes have been approximated using a first-order upwind scheme:

$$\begin{aligned} a_W &= \left[\frac{\Gamma_{\phi,w} A_w}{\delta x_{WP}} \right] + \max(\bar{u}_w A_w, 0), \\ a_E &= \left[\frac{\Gamma_{\phi,e} A_e}{\delta x_{PE}} \right] + \max(-\bar{u}_e A_e, 0), \\ a_S &= \left[\frac{\Gamma_{\phi,s} A_s}{\delta y_{SP}} \right] + \max(\bar{v}_s A_s, 0), \\ a_N &= \left[\frac{\Gamma_{\phi,n} A_n}{\delta y_{PN}} \right] + \max(-\bar{v}_n A_n, 0), \\ a_B &= \left[\frac{\Gamma_{\phi,b} A_b}{\delta z_{BP}} \right] + \max(\bar{w}_b A_b, 0), \\ a_T &= \left[\frac{\Gamma_{\phi,t} A_t}{\delta z_{PT}} \right] + \max(-\bar{w}_t A_t, 0), \end{aligned} \quad (36)$$

where $\delta x_{\overline{WP}} \equiv x_P - x_W$ denotes the distance along the x -coordinate direction from the west neighbor node W to the cell center node P , with analogous definitions for other similar quantities in Equation (36). Finally, the central coefficient a_P is

$$a_P = \sum_{\text{nb}} a_{\text{nb}} + \frac{a_0 \Delta \Omega}{2 \Delta t} - S_P \Delta \Omega. \quad (37)$$

urbanSTREAM employs a fully-located, cell-centered storage arrangement for all transported flow properties as well as for pressure. Furthermore, urbanSTREAM allows two user-selected options for the approximation of the advective fluxes across a cell face; namely, the upwind scheme summarized above and the Upstream Monotonic Interpolation for Scalar Transport (UMIST) scheme [11]. The UMIST scheme is a total variation diminishing (TVD) variant of the higher-order quadratic upwind interpolation for convective kinematics (QUICK) scheme developed originally by Leonard [12] to approximate volume-face fluxes. This second-order scheme for the discretization of the net advective flux through a control volume combines the second-order accuracy of a central differencing scheme with the stability inherent in an upwind differencing scheme by using in each direction separately a quadratic upstream interpolation. The second-order accuracy of the QUICK scheme minimizes numerical diffusion errors that are characteristic of first-order accurate discretization schemes such as the upwind scheme. The UMIST scheme generalizes QUICK by introducing a limiter to give a monotonic version of QUICK that satisfies TVD constraints. In urbanSTREAM, the higher-order advection scheme UMIST is implemented simply as a first-order upwind approximation (described above) augmented with deferred corrections that constitute additional contributions to the source term Q_C given in Equation (35b).

To this purpose, an additional source contribution (deferred corrector ‘source’) Q_C^{DC} is added to Q_C ($Q_C \rightarrow Q_C + Q_C^{\text{DC}}$) in the implementation of UMIST. This deferred corrector source has the following explicit form:

$$\begin{aligned} Q_C^{\text{DC}} = 0.5 \bigg\{ & \left[(\bar{u})_e^+ \vartheta(r_e^+) - (\bar{u})_e^- \vartheta(r_e^-) \right] (\phi_E - \phi_P) \\ & - \left[(\bar{u})_w^+ \vartheta(r_w^+) - (\bar{u})_w^- \vartheta(r_w^-) \right] (\phi_P - \phi_W) \\ & + \left[(\bar{v})_n^+ \vartheta(r_n^+) - (\bar{v})_n^- \vartheta(r_n^-) \right] (\phi_N - \phi_P) \\ & - \left[(\bar{v})_s^+ \vartheta(r_s^+) - (\bar{v})_s^- \vartheta(r_s^-) \right] (\phi_P - \phi_S) \\ & + \left[(\bar{w})_t^+ \vartheta(r_t^+) - (\bar{w})_t^- \vartheta(r_t^-) \right] (\phi_T - \phi_P) \\ & - \left[(\bar{w})_b^+ \vartheta(r_b^+) - (\bar{w})_b^- \vartheta(r_b^-) \right] (\phi_P - \phi_B) \bigg\}, \end{aligned} \quad (38a)$$

where $\vartheta(r)$ is defined as

$$\vartheta(r) \equiv \max \left[0, \min \left(2r, 0.25 + 0.75r, \underbrace{0.75 + 0.25r}_{\text{QUICK}}, 2 \right) \right], \quad (38b)$$

in which the term singled out by the underbrace is the contribution from the QUICK scheme (viz., if $\vartheta(r)$ were exactly equal to the term highlighted by the underbrace in Equation (38b), then the advective flux approximation reduces exactly to Leonard’s QUICK

scheme). Furthermore, in Equation (38a), the following definitions have been used:

$$(\bar{u})^{\pm} = (\bar{u} \pm |\bar{u}|)/2, \quad (\bar{v})^{\pm} = (\bar{v} \pm |\bar{v}|)/2, \quad (\bar{w})^{\pm} = (\bar{w} \pm |\bar{w}|)/2; \quad (39a)$$

and, r_{κ}^{\pm} ($\kappa \in \{w, e, n, s, t, b\}$) are

$$r_e^+ = \frac{\phi_P - \phi_W}{\phi_E - \phi_P}, \quad r_e^- = \frac{\phi_E - \phi_{EE}}{\phi_P - \phi_E}, \quad r_w^+ = \frac{\phi_W - \phi_{WW}}{\phi_P - \phi_W}, \quad r_w^- = \frac{\phi_P - \phi_E}{\phi_W - \phi_P}, \quad (39b)$$

$$r_n^+ = \frac{\phi_P - \phi_S}{\phi_N - \phi_P}, \quad r_n^- = \frac{\phi_N - \phi_{NN}}{\phi_P - \phi_N}, \quad r_s^+ = \frac{\phi_S - \phi_{SS}}{\phi_P - \phi_S}, \quad r_s^- = \frac{\phi_P - \phi_N}{\phi_S - \phi_P}, \quad (39c)$$

$$r_t^+ = \frac{\phi_P - \phi_B}{\phi_T - \phi_P}, \quad r_t^- = \frac{\phi_T - \phi_{TT}}{\phi_P - \phi_T}, \quad r_b^+ = \frac{\phi_B - \phi_{BB}}{\phi_P - \phi_B}, \quad r_b^- = \frac{\phi_P - \phi_T}{\phi_B - \phi_P}, \quad (39d)$$

where EE refers to the node east of node E , WW refers to the node west of node W , and so forth. It is noted that the higher-order UMIST scheme for approximation of advective volume-face fluxes uses a twelve-point molecule, with the neighborhood of a cell center P consisting of W , E , S , N , B , T , WW , EE , SS , NN , BB , and TT .

Pressure-correction algorithm

For an incompressible flow, there is no direct method for specifying an equation for pressure. In this case, pressure needs to be interpreted as a kinematic variable (Lagrange multiplier) which is determined indirectly so as to satisfy the continuity equation [cf. Equation (4)]. Indeed, the lack of a temporal derivative in the continuity equation implies that this equation can be interpreted as a constraint for the pressure (rather than a transport or evolution equation). In urbanSTREAM, the continuity equation is enforced indirectly by solving a pressure-correction equation which, as part of the iterative sequence, steers the pressure towards a state in which all mass residuals in the cells are negligibly small. The two iterative schemes available in urbanSTREAM to enforce mass conservation through a pressure-correction algorithm are the Semi-Implicit Method for Pressure-Linked Equations (SIMPLE) described in detail by Patankar [13] and the SIMPLC (SIMPLE-Consistent) algorithm of Van Doormal and Raithby [14].

The SIMPLE(C) algorithm provides a method for connecting the discretized forms of the momentum and continuity equations to give an equation linking the pressure correction at a node to its neighboring nodes. In this iterative solution sequence, \bar{u}_i ($i = 1, 2, 3$) are initially obtained with an estimated pressure field. This is continuously updated by reference to the local mass residuals, which are used to steer the pressure field towards the correct level. However, the fully collocated variable storage used in urbanSTREAM, in combination with a central differencing for pressure, is known to provoke checkerboard oscillations, reflecting the pressure-velocity decoupling. More specifically, if a linear interpolation scheme is used to determine the pressure on cell faces, the pressure gradient across a cell depends on the pressure at the nodes in the neighboring cells and is independent of the pressure in the current cell, leading to the above mentioned checkerboard pattern in the pressure. To avoid this, the widely used interpolation practice of Rhie and Chow [15] is adopted to interpolate cell-face velocities from the nodal values. This method for interpolation essentially introduces a fourth-order smoothing term based on the pressure, and prevents the occurrence of spurious pressure modes. The interpolation scheme of Rhie and Chow

for removing checkerboard pressure oscillations within a collocated scheme for solving the RANS equations in a generalized curvilinear coordinate system has been presented in detail by Lien and Leschziner [16].

The key concept underlying Rhie and Chow's interpolation for avoidance of checkerboard oscillations in the pressure within a collocated storage arrangement can be seen as follows. To this purpose, let us consider the discretized \bar{u} -momentum transport equation, which by virtue of Equation (35a) [with the identification $\phi \equiv \bar{u}$], is given by

$$\bar{u}_P = \underbrace{\frac{\sum_{nb} a_{nb} \bar{u}_{nb} + Q_C}{a_P}}_{H_P} - (\bar{p}_e - \bar{p}_w) \underbrace{\frac{A_P}{a_P}}_{D_P^{\bar{u}}}, \quad (40)$$

where the discretized pressure gradient term contribution to Q_C has been split out, and A_P is the cross-sectional area of the cell at P . Equation (40) can be re-arranged as follows:

$$\bar{u}_P = H_P - D_P^{\bar{u}}(\bar{p}_e - \bar{p}_w). \quad (41)$$

A corresponding expression can be written for the neighboring node to the east, so

$$\bar{u}_E = H_E - D_E^{\bar{u}}(\bar{p}_{ee} - \bar{p}_e), \quad (42)$$

where ee denotes the eastern face of the cell that has node E at its center. Similarly, the velocity at the eastern face of the cell that has node P at its center is given by

$$\bar{u}_e = H_e - D_e^{\bar{u}}(\bar{p}_E - \bar{p}_P). \quad (43)$$

The critical point to note is that the face velocity \bar{u}_e is evaluated by a linear interpolation of the nodal velocities \bar{u}_P and \bar{u}_E from which then the pressure-gradient terms are subtracted and to which a compensating pressure-gradient fragment is added, the last formed only with the two nodal pressures that straddle the face velocity \bar{u}_e . The result gives

$$\begin{aligned} \bar{u}_e &= \frac{1}{2}(H_P + H_E) - \frac{1}{2}(D_P^{\bar{u}} + D_E^{\bar{u}})(\bar{p}_E - \bar{p}_P) \\ &= \frac{1}{2} \left[\bar{u}_P + D_P^{\bar{u}}(\bar{p}_e - \bar{p}_w) + \bar{u}_E + D_E^{\bar{u}}(\bar{p}_{ee} - \bar{p}_e) \right] - \frac{1}{2}(D_P^{\bar{u}} + D_E^{\bar{u}})(\bar{p}_E - \bar{p}_P), \end{aligned} \quad (44)$$

which can be recast into the following more perspicuous form:

$$\begin{aligned} \bar{u}_e &= \underbrace{\frac{1}{2}(\bar{u}_P + \bar{u}_E)}_{\text{linear interpolation}} \\ &\quad + \underbrace{\frac{1}{2} \left[D_P^{\bar{u}}(\bar{p}_e - \bar{p}_w) + D_E^{\bar{u}}(\bar{p}_{ee} - \bar{p}_e) - (D_P^{\bar{u}} + D_E^{\bar{u}})(\bar{p}_E - \bar{p}_P) \right]}_{\text{pressure smoothing}}. \end{aligned} \quad (45)$$

Equation (45) implies that the Rhie and Chow interpolation practice consists of two parts: a centered approximation for \bar{u}_e and a stabilizing pressure smoothing term which is a function of pressure at the neighboring nodes. Note that \bar{u}_e in Equation (45) depends on the values of pressure at four nodes, two on either side of the cell face.

The pressure-correction equation now arises by decomposing the correct pressure field \bar{p} into an approximate (guessed) pressure field \bar{p}^* and a corrective pressure perturbation \bar{p}' , so that

$$\bar{p} = \bar{p}^* + \bar{p}'. \quad (46)$$

Similarly, the correct face velocity \bar{u}_e is decomposed into an estimated (or, guessed) value \bar{u}_e^* and a correction \bar{u}_e' :

$$\bar{u}_e = \bar{u}_e^* + \bar{u}_e', \quad (47)$$

where $\bar{u}_e' \approx d_e^{\bar{u}}(\bar{p}'_P - \bar{p}'_E)$, with $d_e^{\bar{u}}$ denoting the value of $d^{\bar{u}}$ at cell face e obtained as a centered average of the values of $d^{\bar{u}}$ at the two neighboring nodes on either side of the face (viz., at nodes P and E). The form for $d^{\bar{u}}$ depends on the pressure-based algorithm used. In the SIMPLE algorithm, $d_e^{\bar{u}} = A_e/a_e = D_e^{\bar{u}}$. However, for the SIMPLEC algorithm which provides a better approximation for the corrective velocity perturbation, $d_e^{\bar{u}} = A_e/(a_e - \sum a_{nb})$. Substitution of Equation (47) along with analogous expressions for the other cell face velocities into the continuity equation, and integrating over the volume of a cell, yields the following discretization equation for \bar{p}' :

$$a_P^{\bar{p}} \bar{p}'_P = \sum_{nb} a_{nb}^{\bar{p}} \bar{p}'_{nb} + b^{\bar{p}}, \quad (48)$$

where

$$a_E^{\bar{p}} = d_e^{\bar{u}} A_e, \quad a_W^{\bar{p}} = d_w^{\bar{u}} A_w, \quad (49a)$$

$$a_N^{\bar{p}} = d_n^{\bar{v}} A_n, \quad a_S^{\bar{p}} = d_s^{\bar{v}} A_s, \quad (49b)$$

$$a_T^{\bar{p}} = d_t^{\bar{w}} A_t, \quad a_B^{\bar{p}} = d_b^{\bar{w}} A_b, \quad (49c)$$

and

$$a_P^{\bar{p}} = a_W^{\bar{p}} + a_E^{\bar{p}} + a_S^{\bar{p}} + a_N^{\bar{p}} + a_B^{\bar{p}} + a_T^{\bar{p}}, \quad (49d)$$

with the mass imbalance $b^{\bar{p}}$ given by

$$b^{\bar{p}} = (\bar{u}_w^* A_w - \bar{u}_e^* A_e) + (\bar{v}_s^* A_s - \bar{v}_n^* A_n) + (\bar{w}_b^* A_b - \bar{w}_t^* A_t). \quad (49e)$$

We note that if $b^{\bar{p}}$ vanishes identically, then the starred velocity field satisfies the continuity equation and no pressure correction is needed. The term $b^{\bar{p}}$ can be interpreted as a “mass source” which the pressure corrections must annihilate (through the associated velocity corrections) in order for the continuity equation to be exactly satisfied.

The pressure-correction equation for \bar{p}' is susceptible to divergence unless some under-relaxation is applied during the iterative process. In view of this, only a fraction of \bar{p}' is added to \bar{p}^* in Equation (46) to give the corrected pressure \bar{p} , so that

$$\bar{p} = \bar{p}^* + \alpha_p \bar{p}', \quad (50)$$

where $\alpha_p \in (0, 1]$. For the SIMPLE algorithm, α_p is typically chosen to have a value of about 0.7. However, it is important to note that under-relaxation of the pressure is not required for the SIMPLEC algorithm, so in this case $\alpha_p = 1.0$. Similarly, we also under-relax the corrections for velocity (cf. Equation (47) and analogous expressions for the other velocity components). The under-relaxation of the velocity does not need to be computed directly, but rather it is more convenient (and elegant) to implement this under-relaxation while

solving the discretized equations for \bar{u}_i ($i = 1, 2, 3$). With reference to Equation (35a) with $\phi \equiv \bar{u}_i$, the under-relaxation of the discretized \bar{u}_i -momentum equation takes the following form:

$$\frac{a_P^{\bar{u}_i}}{\alpha_{\bar{u}_i}} \bar{u}_i = \sum_{nb} a_{nb}^{\bar{u}_i} \bar{u}_i + Q_C^{\bar{u}_i} + \left[(1 - \alpha_{\bar{u}_i}) \frac{a_P^{\bar{u}_i}}{\alpha_{\bar{u}_i}} \right] \bar{u}_i^*, \quad (51)$$

where $\alpha_{\bar{u}_i} \in (0, 1]$ is the under-relaxation factor for \bar{u}_i ; and, \bar{u}_i^* is the value of \bar{u}_i from the previous iteration. In Equation (51), the contribution of the pressure gradient term has been absorbed in $Q_C^{\bar{u}_i}$ and the effect of the under-relaxation of the momentum equation is to introduce an additional contribution to the source term. Its effect, therefore, is to increase the diagonal dominance of the coefficient matrix through the inclusion of this additional source term. Finally, we note that the pressure-correction equation is also affected by the under-relaxation of the \bar{u}_i -momentum equations in the sense that the $d^{\bar{u}_i}$ -terms in the pressure-correction equation [cf. Equation (49)] need to be replaced as follows:

$$d^{\bar{u}_i} \rightarrow d^{\bar{u}_i} \alpha_{\bar{u}_i}, \quad i = 1, 2, 3. \quad (52)$$

The solution procedure for the velocity field in urbanSTREAM is as follows. For each time step, the following procedure is undertaken: (a) Guess the pressure field \bar{p}^* and solve the mean momentum equations to obtain the provisional Cartesian velocity components \bar{u}_i^* ($i = 1, 2, 3$); (b) With the provisional velocity \bar{u}_i^* ($i = 1, 2, 3$), solve the pressure-correction equation to obtain \bar{p}' ; (c) Update the provisional velocities and pressure to \bar{u}_i ($i = 1, 2, 3$) and \bar{p} using the velocity-correction and pressure-correction formulae; (d) Solve all the other discretized transport equations (e.g., k and ϵ); (e) Treat the corrected pressure \bar{p} as the new guessed pressure \bar{p}^* ; and, (f) Return to Step (a) until a converged solution is obtained at which point proceed to the next time step.

Within this scheme, the transport equations for \bar{u}_i ($i = 1, 2, 3$), k , and ϵ and the pressure-correction equation are solved sequentially and iterated to convergence, defined by reference to L1-residual norms for the mass and momentum components. Here, the L1-residual norm is defined as the sum of absolute residuals over all grid points of the flow domain. The residual norm provides a quantitative measure of how perfectly the discretization equations are satisfied by the current values of the dependent variables. The L1-residual norms for the mass and momentum components were normalized by the mass and momentum fluxes at the inflow plane. A convergent solution was assumed after each normalized L1-residual norm decreased below 0.001 (although this level for declaration of convergence can be chosen by the user). In urbanSTREAM, the discretized equations are solved using an iterative method called the strongly implicit procedure (SIP) that was proposed by Stone [17]. The SIP method uses an incomplete lower-upper (LU) decomposition and was specifically designed for solving algebraic equations that arise from the discretizations of partial differential equations (e.g., those that arise in various CFD applications). For these types of problems, Stone's SIP method generally converges in a small number of iterations.

Boundary condition implementation

The boundary conditions used in urbanSTREAM (flow solver) and urban(A)EU (urban dispersion) pertain to physical situations described by partial differential equations of either a parabolic or elliptic character. For the mean concentration C and C^* , at all solid boundaries (e.g., ground surface, walls and roofs of buildings, etc.) in the computational domain, zero Neumann conditions were used, implying no flux of C and C^* across the solid boundary (viz., $\partial C/\partial n|_B = 0$ and $\partial C^*/\partial n|_B = 0$ where n refers to the direction normal to the solid boundary B). At the computational (flow) domain boundaries, zero Neuman conditions were applied for C , but convective boundary conditions were used for C^* (viz., $K_{\text{eff}}\partial C^*/\partial n + \mathbf{u} \cdot \mathbf{n}C^* = 0$ where $K_{\text{eff}} \equiv (K + K_t)$ and \mathbf{n} is the unit outward normal vector to the flow domain boundary).²

The boundary conditions imposed on the flow field are more complex. At the inflow boundaries of the computational domain, all transported flow properties need to be prescribed (i.e., Dirichlet boundary conditions apply here). With the velocity prescribed, no boundary conditions are needed for the pressure. In urbanSTREAM, the mean velocity components \bar{u}_i ($i = 1, 2, 3$) and the turbulence kinetic energy k at the inflow boundary planes are provided by urbanGRID which imports four-dimensional (3-space dimensions plus 1-time dimension) meteorological fields from urban GEM LAM and interpolates these field quantities on the grid nodes of the inflow planes. Alternatively, measured profiles of mean velocity and turbulence kinetic energy (e.g., obtained from sodars, radiosondes, radars, etc.) can also be used by urbanSTREAM to define the boundary conditions for mean flow and turbulence on the inflow boundary planes, if these are available. Unfortunately, the viscous dissipation rate ϵ is not available from urban GEM LAM and is virtually never available from experimental measurements. In urbanSTREAM, ϵ is prescribed on the inflow boundary planes using the assumption of local equilibrium of the turbulent flow (so that the rates of production and destruction of turbulence are in near balance) to give

$$\epsilon = \frac{C_\mu^{3/4} k^{3/2}}{\min(k_v z, h/3)}, \quad (53)$$

where z is vertical distance from the ground and h is the atmospheric boundary-layer height³.

Far downstream, at the outflow boundary planes, the flow was assumed to reach a fully-developed state where no changes occur in the flow direction (approximately or better). Hence, at the outflow boundary, the horizontal gradients of all flow variables are assumed to be zero; viz., $\partial \bar{u}/\partial x_i = \partial \bar{v}/\partial x_i = \partial \bar{w}/\partial x_i = \partial k/\partial x_i = \partial \epsilon/\partial x_i = 0$ ($i = 1, 2$). At the upper boundary, we used free-slip conditions for all flow variables. Furthermore, at the outflow boundaries, a mass flux correction is undertaken to ensure that the total mass flux that exits through the outflow boundary planes is equal to the total mass flux that enters through the inflow boundary planes (and, in fact, the imposition of this condition enhances convergence of the iterative flow solver). During iterations of the pressure-based algorithm

² The convective boundary conditions need to be used for C^* to ensure that C^* is the adjoint of C , verifying the duality relationship of Equation (31).

³ The upper limit of $h/3$ in the turbulence length scale used in Equation (53) is consistent with that used in the limited-length-scale k - ϵ turbulence model.

(either SIMPLE or SIMPLEC), there is no guarantee that the exit velocities through the outflow boundary planes will conserve mass over the computational domain as a whole. To ensure that the continuity is satisfied globally, the total mass flux $M_{\text{in}}^{x_i}$ entering into the domain and total mass flux $M_{\text{out}}^{x_i}$ going out of the domain in the x_i -coordinate direction ($i = 1, 2$) are first calculated as follows:

$$M_{\text{in}}^{x_i} = \sum_{j \in \mathcal{I}^{x_i}} (\bar{u}_i)_j \Delta A_j; \quad M_{\text{out}}^{x_i} = \sum_{j \in \mathcal{O}^{x_i}} (\bar{u}_i)_j \Delta A_j, \quad i = 1, 2, \quad (54)$$

where \mathcal{I}^{x_i} and \mathcal{O}^{x_i} denote the inflow and outflow boundary planes normal to the x_i -coordinate direction, respectively; and, $(\bar{u}_i)_j$ corresponds to the inlet (exit) velocity through inlet (exit) cell j whose inlet (exit) face area is ΔA_j . There is no unique procedure for ensuring that the mass flux out $M_{\text{out}}^{x_i}$ is equal to mass flux in $M_{\text{in}}^{x_i}$ for $i = 1, 2$. One method to ensure overall continuity is to add a constant velocity correction \bar{u}_i^c given by

$$\bar{u}_i^c = \frac{(M_{\text{in}}^{x_i} - M_{\text{out}}^{x_i})}{\sum_{j \in \mathcal{O}^{x_i}} \Delta A_j}, \quad i = 1, 2, \quad (55)$$

to the outlet velocity component $(\bar{u}_i)_j$, $j \in \mathcal{O}^{x_i}$ ($i = 1, 2$). Alternatively, global continuity in the computational domain can also be ensured by multiplying the outflow plane velocities $(\bar{u}_i)_j$ ($j \in \mathcal{O}^{x_i}$) by the ratio $M_{\text{in}}^{x_i}/M_{\text{out}}^{x_i}$. Currently, urbanSTREAM uses the first method for ensuring that mass is conserved over the entire computational domain.

At all the solid boundaries (ground, obstacle walls, obstacle roofs), standard wall functions are applied for the mean velocities and turbulence quantities. Wall functions are used to reduce the computational cost associated with the alternative of using a low-Reynolds number turbulence model to numerically integrate the solution through the entire near-wall region, including the viscous sublayer up to the wall where no-slip and impermeability conditions can be applied. Typically, this will require a very fine grid near the wall because spatial variations in near-wall turbulence structure are large here due to the combined influence of viscosity and wall-induced anisotropy. Log-law based ‘wall laws’ are adopted in conjunction with high-Reynolds number turbulence models to bridge the viscous sublayer. Basically, the flow quantities at the first grid point above the solid surface, which is located outside the viscous sublayer, are related to the wall friction velocity based on the assumption of a semi-logarithmic velocity distribution.

The implementation of a wall function boundary condition for the mean velocity tangential to the wall first requires the evaluation of the normalized distance perpendicular to the wall:

$$z^+ = \frac{z_P}{\nu} \left(\frac{\tau_w}{\rho} \right)^{1/2}, \quad (56)$$

where z_P is the distance from the near-wall node P to the solid surface, τ_w is the wall shear stress, and ρ is fluid density. If $z^+ \leq 11.6$, the flow at near-wall node P is assumed to be in the laminar sublayer where the flow is linear; otherwise, the flow is turbulent, lying in the log-law region where a log variation in the tangential velocity is assumed to prevail and a wall function is used. For the velocity component \bar{u}_3 normal to the wall, the impermeability condition that $\bar{u}_3 = 0$ at the wall is used.

More specifically, if $z^+ \leq 11.6$, the wall shear stress in the x_i -coordinate direction ($i = 1, 2$) is obtained from $\tau_w^{x_i} = \rho\nu(\bar{u}_i)_P/z_P$, where $(\bar{u}_i)_P$ is the tangential velocity at the near-wall node P (assuming a linear variation of velocity with distance from the wall). The shear force F_s on the bottom face of the near-wall cell (with center node P) is given by $F_s = -\rho\nu(\bar{u}_i)_PA_b/z_P$ (A_b is the wall (bottom) area of the near-wall cell). The link to the wall in the discretized \bar{u}_i -momentum equation ($i = 1, 2$) is suppressed by setting $a_B = 0$ and the wall function contribution $S_P^{wf} = -\rho\nu A_b/z_P$ is added to S_P [cf. Equation (37)]. If, however, $z^+ > 11.6$, the near-wall node P is considered to lie in the log-law region of the turbulent flow and a wall function is utilized. To this purpose, one calculates the wall shear stress τ_w and the associated wall shear force F_s from the log-law velocity profile with properties evaluated at the near-wall node P . Again, the coefficient a_B in the discretized \bar{u}_i -momentum equation ($i = 1, 2$) is nullified and the source Q_C [cf. Equation (35b)] is modified to explicitly include the contribution from the shear force acting on the bottom near-wall cell face as follows:

$$Q_C \rightarrow Q_C - \frac{\rho k_P^{1/2} C_\mu^{1/4} k_v}{\ln(Ek_P^{1/2} z_P/\nu)} (\bar{u}_i)_P A_b, \quad i = 1, 2, \quad (57)$$

where $E = 9.793$ is a constant.

To implement the wall function of Equation (57), a correct value for k_P (TKE at the near-wall node) is required. A local equilibrium of turbulence (where the volume-averaged production and dissipation of turbulence are in balance) is assumed to prevail near the wall. The average production of k in a near-wall cell is given by

$$\overline{P_k} = |\tau_w| \cdot |\mathbf{u}_P^t|/z_P, \quad (58)$$

where $|\tau_w| = ((\tau_w^{x_1})^2 + (\tau_w^{x_2})^2)^{1/2}$ and $|\mathbf{u}_P^t| \equiv ((\bar{u}_1)_P^2 + (\bar{u}_2)_P^2)^{1/2}$ are the magnitudes of the wall shear stress and the tangential velocity (at near-wall node P), respectively. With respect to implementation, the net k -source per unit volume in Equation (58) is included in the near-wall cells in the discretized k -transport equation by suppressing the link to the wall boundary ($a_B = 0$) and augmenting the source term Q_C with the additional contribution $Q_C^{\text{prod}} = |\tau_w| \cdot |\mathbf{u}_P^t| \Delta\Omega/z_P$ ($\Delta\Omega$ is the volume of the near-wall cell). Finally, the viscous dissipation ϵ at a near-wall cell with center node P has the nodal value set at (with an assumed local equilibrium condition persisting in the near-wall cell)

$$\epsilon_P = C_\mu^{3/4} k_P^{3/2} / (k_v z_P). \quad (59)$$

Application to real urban environment

Here, a computational study is performed in which the capabilities of urbanSTREAM for urban flow prediction and urban(A)EU for urban dispersion predictions are examined by reference to a full-scale experimental study of flow and dispersion in a real cityscape (Oklahoma City, Oklahoma).

Joint Urban 2003

Joint Urban 2003 (JU2003) experiment was a major urban study that was conducted in Oklahoma City, Oklahoma during the period from June 28 to July 31, 2003 [18]. The principal objective of JU2003 was to obtain high-quality meteorological and tracer data sets documenting urban flow and dispersion in a real city on a range of scales: namely, from flow and dispersion in and around a single city block (street canyon at building scale), to that in and around several blocks in the central business district (CBD) of downtown Oklahoma City (neighborhood scale), and finally to that in the suburban area several kilometers from downtown Oklahoma City (urban scale). Additionally, JU2003 included measurements of indoor flow and dispersion in four buildings in the CBD that were coordinated and conducted in conjunction with the outdoor urban field experiments in order to study physical mechanisms involved in indoor-outdoor exchange rates.

A large number of meteorological measurements in Oklahoma City were obtained during JU2003. These included detailed measurements of wind and turbulence characteristics in the urban atmospheric boundary layer obtained with remote sensing instruments such as Doppler lidars, Doppler sodars (acoustic wind profiler) and radar profilers; and, measurements of wind, temperature, and turbulence in the urban canopy layer (including, within a street canyon) using fast-response in-situ meteorological sensors such as sonic anemometers and infrared thermometers. Furthermore, tracer bag samplers were used to measure mean concentration data obtained from the release of a sulfur hexafluoride (SF_6) tracer in downtown Oklahoma City, Oklahoma at three different locations. To this purpose, ten intensive observation periods (IOPs) were undertaken during JU2003, during each of which there was typically three 30-minute (continuous) tracer gas releases as well as four puff (instantaneous) releases where balloons filled with tracer gas were “popped”. For all the IOPs, each of the three 30-minute continuous releases was separated by 90 minutes and this set of three continuous releases was either preceded or followed by a set of four instantaneous releases with a 20-minute interval between each release. The release rates for the continuous source was constant (generally to within about 5%) during each experiment, and the release rates from the various experiments ranged over the interval from $2\text{--}5\text{ g s}^{-1}$. The tracer masses released from the instantaneous source varied over the range from 300–1000 g. The tracer gas from all releases was sampled in and around downtown Oklahoma City on the regular CBD sampler grid and as far downwind as four kilometers from the release along various sampling arcs. The first six IOPs were conducted during the day from 08:00 CST to 16:00 CST, whereas the last four IOPs were conducted during the night from 22:00 CST to 06:00 CST.

Grid generation for Oklahoma City

Some capabilities of the modeling system are presented with the aid of numerical simulations performed for a built-up (urban) region in Oklahoma City, Oklahoma. The modeling domain with the extent of $1,934.25\text{ m} \times 3,610.6\text{ m} \times 800.0\text{ m}$ in the x - (or, W-E), y - (or, S-N) and z - (or, vertical) directions, respectively, covers the CBD of Oklahoma City and surrounding environs. At ground level where $z = 0$, the southwest corner of the modeling domain (see Figure 6) is at the following coordinates in the Universal Transverse Mercator (UTM) coordinate system⁴: zone = 14, $x_0 = 633,683$ UTM easting and $y_0 = 3,923,940$ UTM

⁴ The UTM easting coordinate reported here and elsewhere in this report is referenced relative

northing (or, equivalently, in the geodetic coordinate system this location is 35.449959° N and -97.52694° E). The internal coordinate system used in urbanSTREAM is shown in Figure 6, where the southwest corner of the modeling region is chosen as the origin (0, 0) in the x - y (horizontal) plane. All distances shown here have been normalized by a reference length scale which is chosen in this case to be $\Lambda_{\text{ref}} = 644.75$ m. Hence, in this internal coordinate system, the northeast corner of the modeling region is referenced as (3, 5.6). A proper subset within this modeling region is chosen as the region in which buildings will be explicitly resolved in the flow simulation; for this example, this rectangular building-aware region ($644.75 \text{ m} \times 709.23 \text{ m}$) has its southwest corner at (1, 2.5) and its northeast corner at (2, 3.6). In the portion of the modeling region lying outside the building-aware region, all buildings are treated as virtual and their effects on the flow are modeled using a distributed drag force representation in the mean momentum equations.

ESRI Shapefiles of the shapes, locations and heights of buildings in Oklahoma City are available from the Joint Urban 2003 archival database (<https://ju2003-dpd.dpg.army.mil>). These Shapefiles were used in urbanGRID to generate automatically a grid mesh over the modeling region as shown in Figure 7. The simulation was carried out in a three-dimensional Cartesian framework, and curved surfaces on buildings or planar building surfaces that are not aligned with the grid lines are approximated by stepwise surfaces. A mesh of $99 \times 139 \times 69$ grid lines in the x -, y -, and z -directions, respectively, was used to accommodate all the necessary geometrical details. The interior building-aware region was covered with a fine calculation grid of $55 \times 100 \times 69$ grid lines to better approximate the building features in this region. The grid arrangement adopted here is shown in the x - y plane in Figure 7. Hence, the fine grid used for the building-aware region contains 379,500 nodes, whereas the entire computational domain was covered with a mesh of 945,509 nodes. The grid lines were preferentially concentrated near the solid surfaces (ground, building rooftops and walls) where the gradients in the flow properties are expected to be greatest, and the spacing between the grid lines was gently stretched with increasing distance from the solid surfaces. Figure 7 shows the finite-volume approximation of the explicitly resolved buildings in the building-aware region, and these approximated buildings should be compared to the actual (true) buildings in this area given in Figure 8 in the form of a satellite photograph and a three-dimensional computer rendering of the buildings from the ESRI Shapefile. As can be seen, there is very little difference between finite volume approximated buildings and the actual (true) buildings and therefore the stepwise approximation of the building surfaces is not expected to undermine the accuracy of the subsequent flow simulation.

Flow field

The flow field in the computational domain was computed using urbanSTREAM in a stand-alone mode (viz., this flow model was not coupled to the urban GEM LAM model). In consequence, at the inflow (inlet) boundary of the computational domain, the measured profiles of the undisturbed mean velocity and turbulence kinetic energy are used. The flow simulation conducted here was for IOP-9 for the time period from 06:00–06:30 UTC (01:00–01:30 CDT) on 28 July 2003 when the prevailing winds were from the south at about 6.8 m s^{-1} at 50-m above ground level at the southern edge of the computational domain shown in Figure 6. As a result, the inflow mean velocity and turbulence kinetic energy profiles (required for the inflow specification) were obtained from the Scintec Multi-

to the central meridian of the zone.

frequency Flat Array Antenna Series (MFAS) sodar operated by a team of investigators from Pacific Northwest National Laboratory (PNNL). The Scintec MFAS sodar has an operating frequency in the 2 kHz band allowing for a spatial resolution of 10 m with a measurement range of up to 1000 m. This sodar was located 2 km south of the central business district of Oklahoma City in a parking lot at the Traffic Maintenance Yard (latitude 35.45° N; longitude -97.53° E) which is on the south edge of Wheeler Park. The area south of this sodar was covered with low-rise (less than three stories) buildings, houses, and trees. The PNNL sodar was located very near the upwind (southern) edge of the computational domain, and measurements of mean wind velocity and turbulence were used to define the inflow conditions for urbanSTREAM.

The flow simulation in the computational domain was carried out using urbanSTREAM in the unsteady RANS mode. The effects of the buildings outside the building-aware region were represented by a distributed drag force approximation in the mean momentum equation with a normalized drag coefficient of $C_d \equiv \hat{C}_d \hat{A} \Lambda_{\text{ref}} = 100$ (where Λ_{ref} is the reference length scale). For the simulations, a constant time step $\Delta t = 30$ s was used. The predicted wind statistics were averaged over 500 time steps after the flow had achieved a (pseudo) steady state. We compared the predicted vertical profiles of the mean horizontal wind speed with associated measured values obtained at three different locations in the computational domain. These comparisons are shown in Figure 9. The measurements of wind speed were obtained from three different sodars: two minisodars deployed by Argonne National Laboratory (ANL) and one sodar operated by National Atmospheric and Oceanic Administration (NOAA) Atmospheric Research Laboratory Field Research Division (ARLFRD). One ANL minisodar was located near the southern edge of the central business district in the Oklahoma City Botanical Garden (latitude 35.46° N; longitude -97.52° E). The CBD of Oklahoma City, which includes many high-rise buildings, was immediately north of this sodar. The second ANL sodar was located approximately 1 km north of the CBD of Oklahoma City near the Minor building (latitude 35.48° N; longitude -97.52° E). The ARLFRD sodar (Radian 600PA phased-array Doppler sodar) was located about 1.5 km northeast of the CBD of Oklahoma City at the campus of the Oklahoma School of Science and Mathematics on the southwest corner of Lincoln and NE 13th Street (latitude 35.48147° N ; longitude -97.5051° E). Both ANL minisodars were operated with the first range gate at 5 m, a range gate spacing of 5 m with the top gate at 200-m above ground level (AGL), and an averaging (integration) time of 15 min. The ARLFRD sodar was operated with the first range gate at 40 m, a range gate spacing of 10 m with the top gate at 300-m AGL, and an averaging (integration) time of 15 min.

From Figure 9, it is seen that the model with the inclusion of the drag force representation for virtual buildings (dashed curves) correctly reproduces the overall qualitative trends in the horizontal wind speeds at the three locations in the computational domain. At the locations of the ANL minisodars, the wind speeds predicted by the model were slightly larger than the measured wind speeds over most of the range between about 25 m and 200 m AGL. The predicted wind speeds agreed well with those measured at the location of the ARLFRD sodar, although the measurements here from one 15-min averaging period to another showed greater variability than those measured at the two ANL minisodar locations. Figure 9 also shows model predictions of horizontal wind speed without the inclusion of a distributed drag force approximation for the virtual buildings (solid lines). Note in this case that the wind speed is greatly overestimated by the model owing to the fact that without a distributed mean-momentum sink within the urban canopy to represent the effects of the

unresolved buildings on the flow, there cannot be a deceleration of the flow in this region leading to the overprediction of the wind speed.

Urban dispersion

The flow field statistics predicted by urbanSTREAM were next used to “drive” an urban dispersion model in both the source-oriented (urbanEU) and receptor-oriented (urbanAEU) modes within the Eulerian framework. Furthermore, these wind field statistics were also used to “drive” a first-order Lagrangian Stochastic (LS) model for urban dispersion (urbanLS, or more precisely urbanLS-1). The simulations were conducted for the second continuous 30-min release of SF₆ in IOP-9, which occurred in the period from 06:00–06:30 UTC (01:00–01:30 CDT) on 28 July 2003. The SF₆ tracer gas was released at a point from a specially designed gas dissemination system that included a mass flow controller attached to a Campbell Scientific CR-23 data logger [19]. The dissemination point was located on the south side of Park Avenue (latitude 35.4687° N; longitude –97.5156° E) with a release height of 1.9 m. This source location was near the center of the computational domain (see Figure 6). The constant gas release rate for this experiment was 2.0 g s^{–1}.

The SF₆ plume concentrations were measured using Programmable Integrating Gas Samplers (PIGS) deployed by ARLFRD. The subsequent analysis of the samples was performed using an Automated Tracer Gas Analysis System (ATGAS) which used gas chromatography (GC) analysis techniques along with autosampler capabilities to give time-integrated concentration measurements. The sampling system was designed to provide average SF₆ plume concentrations over specific time intervals at given receptor locations. The PIGS collected 12 samples by pumping air into 12 individual Tedlar bags. Subsequently, the bag samples were analyzed using the ATGAS. The grid of sampling stations at which predictions of SF₆ plume concentrations were compared with measurements is shown in Figure 10 in relation to the location of the source. The samplers used for comparison include 19 samplers located on the CBD sampling grid and six samplers located along the 1-km sampling arc.

Figure 11 displays various isopleths (on a logarithmic scale) of the predicted mean concentration field C at ground level in the computational domain obtained using urbanEU (source-oriented approach). Figure 12 shows isopleths (on a logarithmic scale) of the influence function C^* (viz., adjunct of the concentration C) at ground level corresponding to one of the sampling locations (receptors) along the 1-km sampling arc. This result was obtained using urbanAEU (receptor-oriented approach). The influence function C^* characterizes the concentration “seen” at the given receptor through the duality relationship of Equation (31) for an arbitrary source distribution Q . In essence, the value of C^* at a given spatial position provides information on the contribution of a point source with a unit emission rate to the concentration at the receptor.

Figure 13 compares predictions of the mean concentration [in parts-per-trillion by volume (pptv)] obtained using urbanEU, urbanAEU and urbanLS-1 with the experimental concentration data measured at 10 different sampling locations along Kerr Avenue and McGee Avenue. Similarly, Figure 14 shows comparisons of mean concentration obtained using the three dispersion models with experimental concentration measurements made at eight sampling stations located along 4th Street and 5th Street. Finally, Figure 15 exhibits predicted and observed mean concentration obtained at two sampling locations along 6th Street and

six sampling stations along the 1-km sampling arc. The experimental concentration data shown here is for a 30-min averaging time. Generally speaking, the predictions for mean concentration at or near the mean plume centerline were quite good, with predictions within a factor of two of the observed concentration. However, the predicted concentrations at sampling locations 56, 66, and 76 were more than a factor of five lower than the experimentally measured values, suggesting that either the predicted plume was too narrow or the eastern edge of the predicted plume was too far west at these locations. Furthermore, it is interesting to note that the 30-min average concentration at the receptor calculated using the influence function (receptor-oriented approach) generally agrees well with the concentration predicted using the source-oriented approach. The discrepancy in the predictions using these two approaches is due to the non-uniform grid utilized in the simulations (the mesh was finer in the region surrounding the source and coarser generally in the region downwind of the source where the receptors were located).

Conclusions

This report provides a technical description of the models that comprise Component 1 of CRTI Project 02-0093RD whose principal objective is the development of an advanced, fully validated, state-of-the-science modeling system for the prediction of urban flow (i.e., turbulent flow through cities) and the concomitant problem of modeling the dispersion of CBRN agents released in a populated urban complex. Component 1 focuses on the development of an urban microscale building-aware flow model and Eulerian-based urban dispersion models. This capability has been developed because almost all current dispersion models employ simple diagnostic wind fields and Gaussian diffusion techniques to predict plume (cloud) dispersion which are not applicable in the highly disturbed flows present in an urban environment.

The principal module of Component 1 is urbanSTREAM, which is a general second-order accurate finite-volume code designed for the simulation of urban flow using a two-equation turbulence closure model (namely, the standard k - ϵ model and limited-length-scale k - ϵ model). This is perhaps the simplest complete turbulence model (in the sense that no advance knowledge of any property of the turbulence is required for the simulation other than the initial and/or boundary conditions for the problem) that is available currently as a general purpose simulator for urban flows. The modeling scheme used here is simple enough to be tractable numerically and, hence, not require excessive computing time which is important if the system is to be employed for emergency response applications. In addition, Component 1 incorporates a module (urbanGRID) for the automatic generation of grids in the computational domain when provided with detailed geometric information on the shapes and locations of buildings in the urban environment in the form of ESRI Shapefiles. Finally, Component 1 also includes modules for the prediction of urban dispersion in the Eulerian framework: namely, urbanEU which is an Eulerian grid dispersion model based on numerical solution of a K -theory advection-diffusion equation (source-oriented approach) and urbanAEU which is a receptor-oriented dispersion model based on numerical solution of the adjoint of the K -theory advection-diffusion equation.

The microscale urban flow and dispersion modeling system of Component 1 has been applied in stand-alone mode to simulate flow and SF₆ tracer dispersion in Oklahoma City, Oklahoma. The numerical simulations of IOP-9 in the Joint Urban 2003 experiment pro-

vide an initial demonstration that the developed modeling system can correctly reproduce many features of the flow and dispersion in a real cityscape. While the results from this preliminary case study are certainly not definitive, they do suggest that the urban dispersion modeling system has the potential to improve the predictive performance capabilities for emergency response in built-up areas where the flow is highly disturbed.

The numerical models included in Component 1 require further improvements and evaluation against data from full-scale meteorological and dispersion field experiments in the urban environment. In particular, an evaluation of the predictive performance of the urban microscale flow and dispersion models when fully coupled with urban GEM LAM will be required. An improvement of the modeling system developed under Component 1 can be expected from: (a) the inclusion of more sophisticated turbulence closure schemes (e.g., second-moment closure which potentially can reproduce effects of streamline curvature, rotation and swirl, secondary motion, and other effects in highly disturbed complex flows better than with an eddy-viscosity concept); (b) application of hybrid Reynolds-averaged Navier-Stokes/large-eddy simulation (RANS/LES) approach which allows very large, coherent, or deterministic structures in the urban flow to be resolved rather than modeled; (c) inclusion of thermal effects on flow and contaminant dispersion in the urban street canyons; and, (d) inclusion of an adaptive mesh refinement capability in the models that would allow a dynamic tracking of the urban flow features as the computation proceeds, giving complete control of grid resolution with an expected concomitant computational savings over a static grid approach. However, we emphasize that these future developments must adhere to the underlying requirement for maintaining a well-balanced compromise between sophistication of mathematical modeling and availability of computational resources.

References

1. ESRI (1998). ESRI Technical Shapefile Technical Description: An ESRI White Paper – July 1998. ESRI, 380 New York Street, Redlands California, USA.
2. Shapelib C Library V1.2. <http://shapelib.maptools.org>.
3. Schewchuk, J. R. (1996). Adaptive Precision Floating Point Arithmetic and Fast Robust Geometric Predicates. Technical Report, School of Computer Science, Carnegie Mellon University, Pittsburgh, PA.
4. Edelsbrunner, H. and Mücke, E. P. (1990) Simulation of Simplicity: A Technique to Cope With Degenerate Cases in Geometric Algorithms. *ACM Trans. Graph.*, 9, 66–104.
5. Launder, B. E. and Spalding, D. B. (1974). The Numerical Computation of Turbulent Flows. *Comp. Meth. Appl. Mech. Eng.*, 3, 1112–1128.
6. Apsley, D. D. and Castro, I. (1997). A Limited-Length-Scale k - ϵ Model for the Neutral and Stably-Stratified Atmospheric Boundary-Layer. *Boundary-Layer Meteorol.*, 83, 75–98.
7. Townsend, A.A. (1980). *The Structure of Turbulent Shear Flows*, Cambridge University Press, Cambridge, England.
8. Lien, F. S., Yee, E. and Wilson, J. D. (2005). Numerical Modeling of the Turbulent Flow Developing Within and Over a 3-D Building Array, Part II: A Mathematical Foundation for a Distributed Drag Force Approach. *Boundary-Layer Meteorol.*, 114, 245–285.
9. Daly, B. J. and Harlow, F. H. (1970). Transport Equations of Turbulence. *Phys. Fluids*, 13, 2634–2649.
10. Wilson, J. D. (2006). User’s Manual and Performance Report for Lagrangian Stochastic Model (‘urbanLS’) for Transport and Mixing of a Hazard Gas in the Urban Environment. J. D Wilson & Associates, Edmonton, Alberta.
11. Lien, F. S. and Leschziner, M. A. (1994). Upstream Monotonic Interpolation for Scalar Transport with Applications to Complex Turbulent Flows. *Int. J. Numer. Methods Fluids*, 19, 527–548.
12. Leonard, B. P. (1979). A Stable and Accurate Convective Modeling Procedure Based on Quadratic Upstream Interpolation. *Comp. Meth. Appl. Mech. Eng.*, 19, 59–98.
13. Patankar, S. V. (1980). *Numerical Heat Transfer and Fluid Flow*, Hemisphere Publishing Corporation, New York.
14. Van Doormal, J. P. and Raithby, G. D. (1984). Enhancements of the SIMPLE Method for Predicting Incompressible Fluid Flows. *Numer. Heat Transfer*, 7, 147–163.
15. Rhie, C. M. and Chow, W. L. (1983). Numerical Study of the Turbulent Flow Past an Airfoil With Trailing Edge Separation. *AIAA J.*, 21, 1525–1532.
16. Lien, F. S. and Leschziner, M. A. (1994). A General Non-Orthogonal Collocated Finite-Volume Algorithm for Turbulent Flow at all Speeds Incorporating Second Moment Closure, Part 1, Computational Implementation. *Comp. Meth. Appl. Mech. Eng.*, 114, 123–148.
17. Stone, H. L. (1968). Iterative Solution of Implicit Approximations of Multidimensional Partial Differential Equations. *SIAM J. Numer. Anal.*, 5, 530–558.

18. Allwine, K. J., Leach, M. J., Stockham, L. W., Shinn, J. S., Hosker, R. P., Bowers, J. F. and Pace, J. C. (2004). Overview of Joint Urban 2003 – An Atmospheric Dispersion Study in Oklahoma City. Symposium on Planning, Nowcasting, and Forecasting in the Urban Zone. Seattle, Washington: American Meteorological Society.
19. Clawson, K. L., Carter, R. G., Lacroix, D. J., Hukari, N. F. and Allwine, K. J. (2004) Joint Urban 2003 Vertical SF₆ Real-Time Analyzer and Time-Integrated Sampler Data Characteristics. Fifth Conference on Urban Environment. Vancouver, British Columbia: American Meteorological Society.

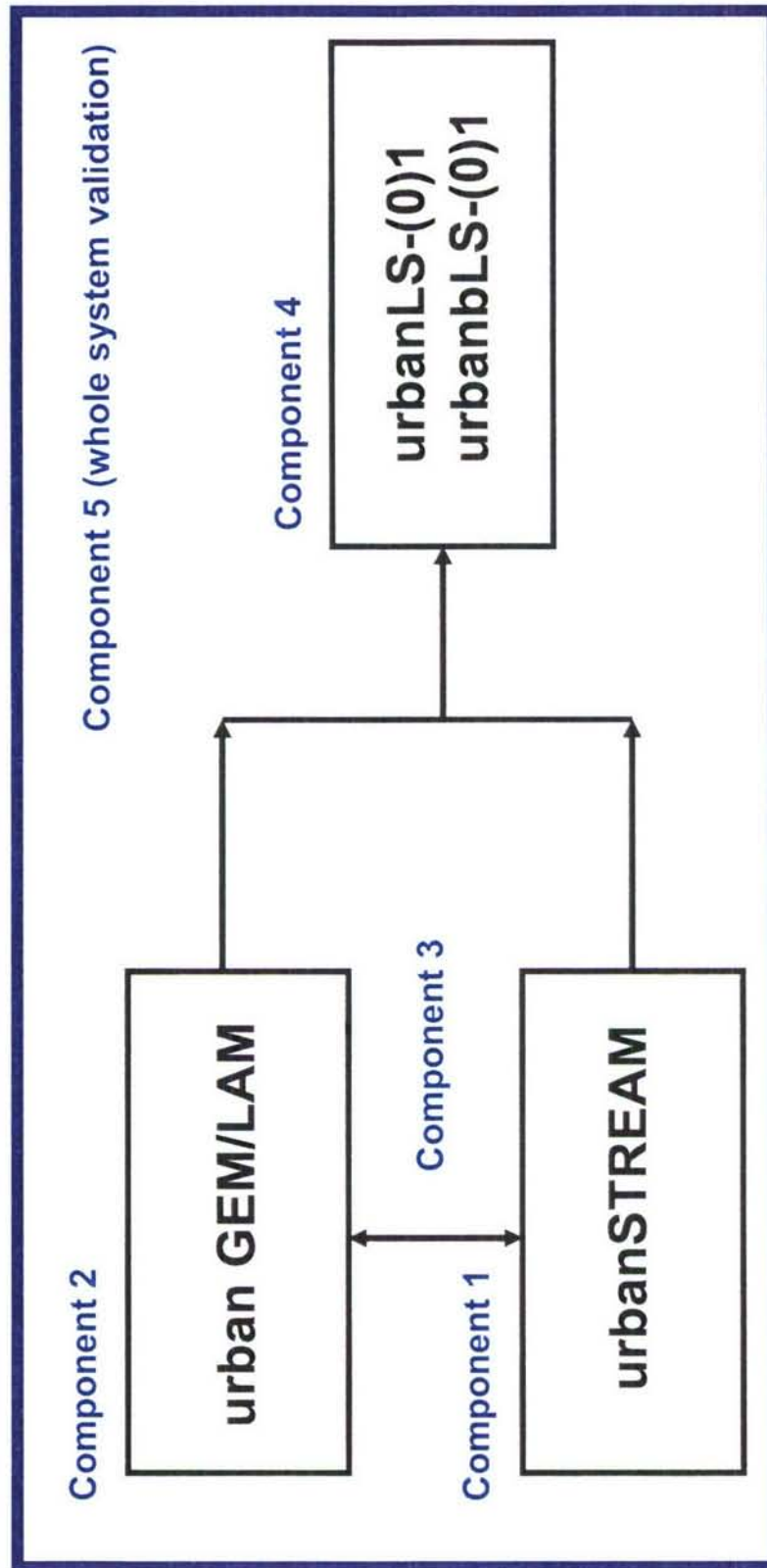


Figure 1. Relationship between various components of CRTI Project 02-0093RD.

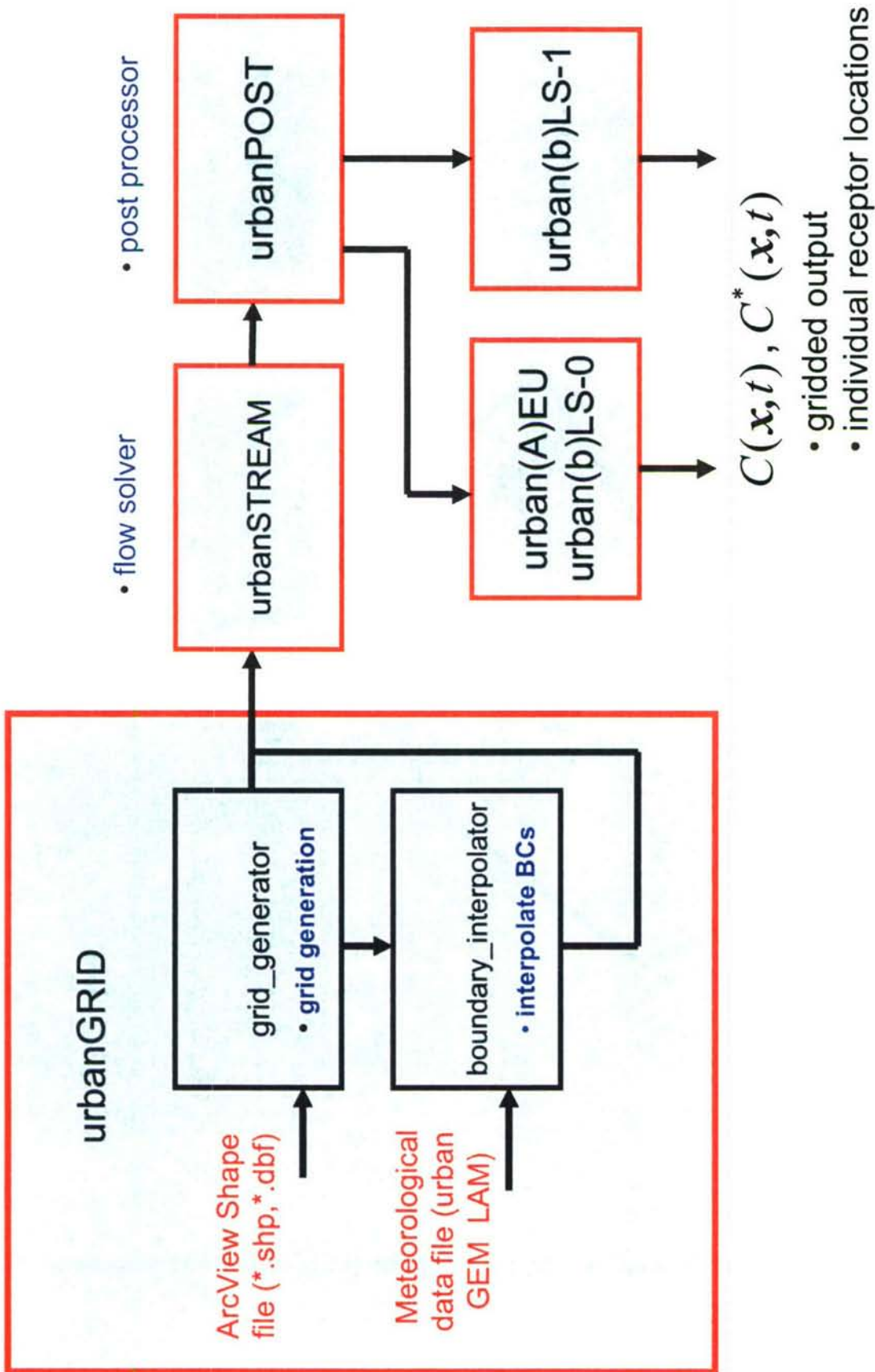


Figure 2. Various modules of Component 1 and their relationship to other components of CRTI Project 02-0093RD.

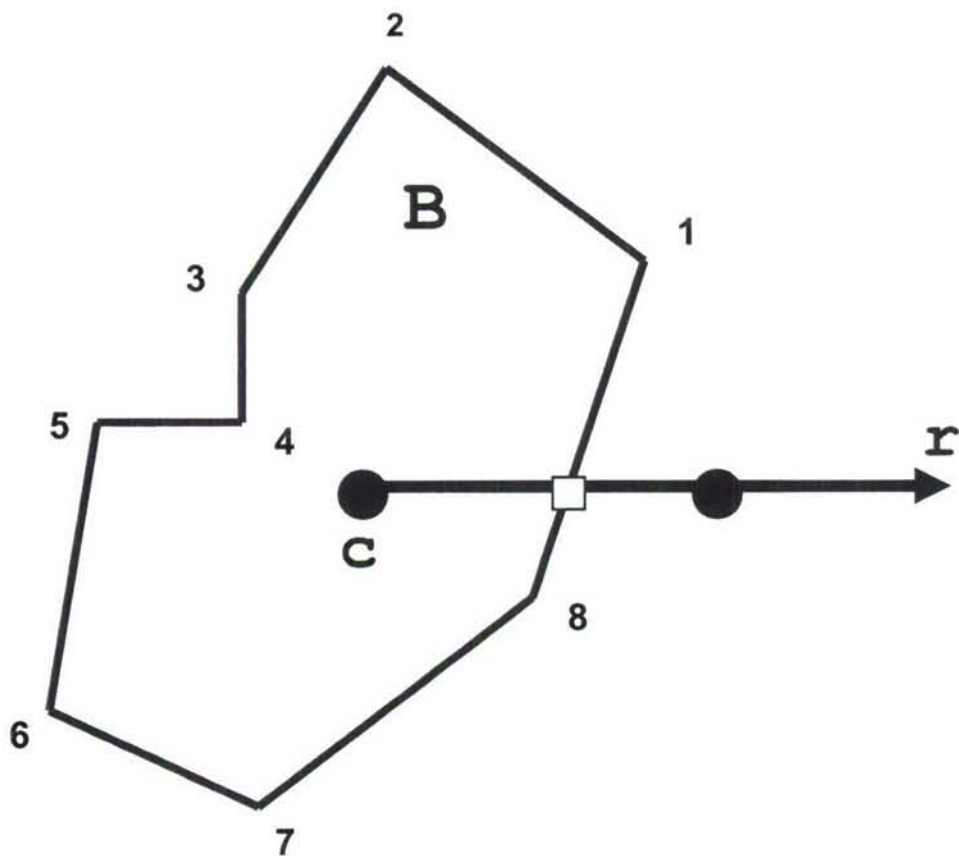


Figure 3. Illustration of the ray-casting approach to determine if a grid cell with centroid c lies inside the building B .

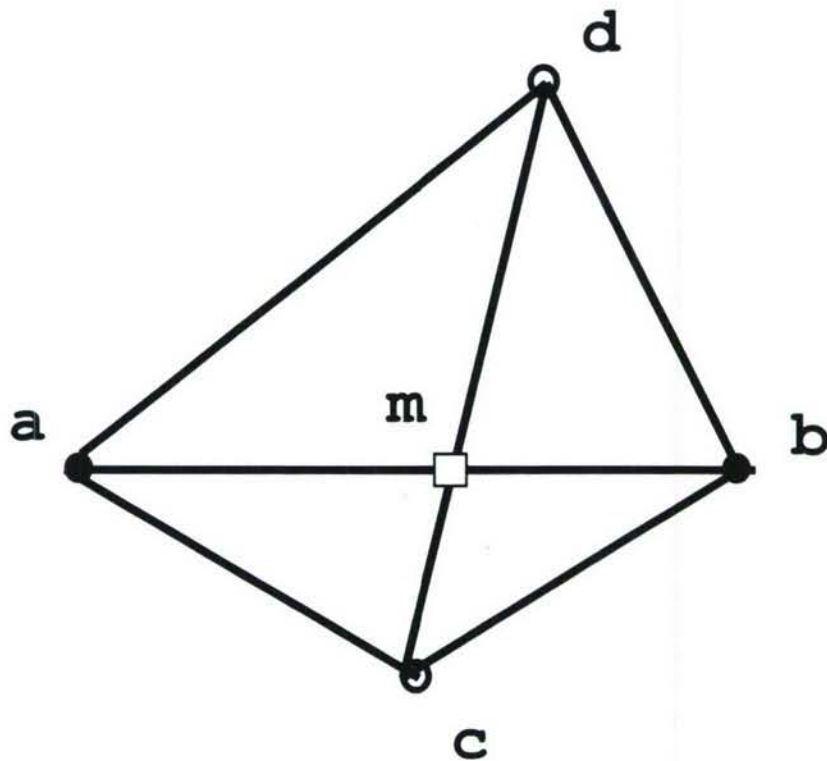


Figure 4. Determination of whether two line segments intersect each other.

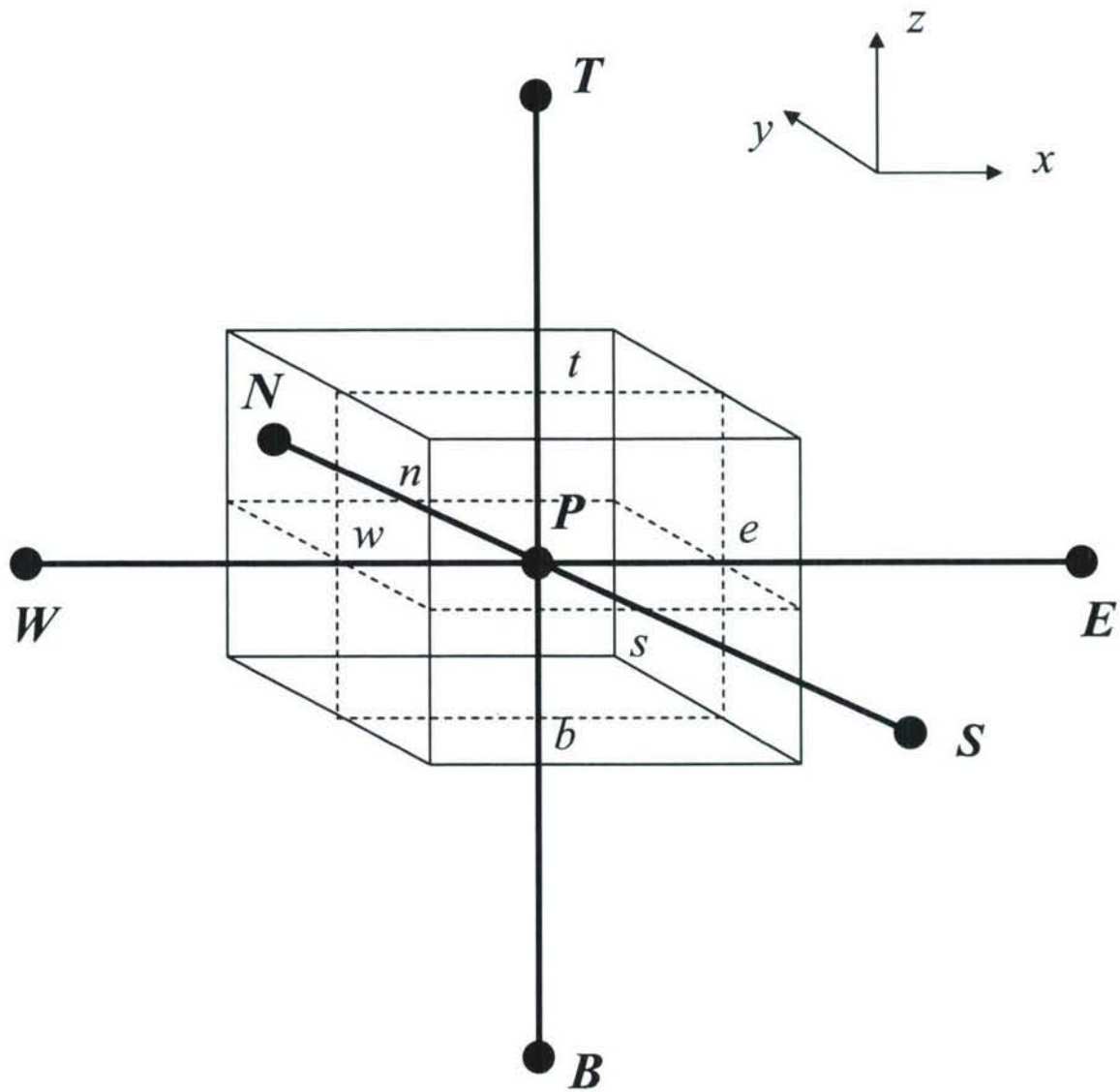


Figure 5. Finite volume and storage arrangement.

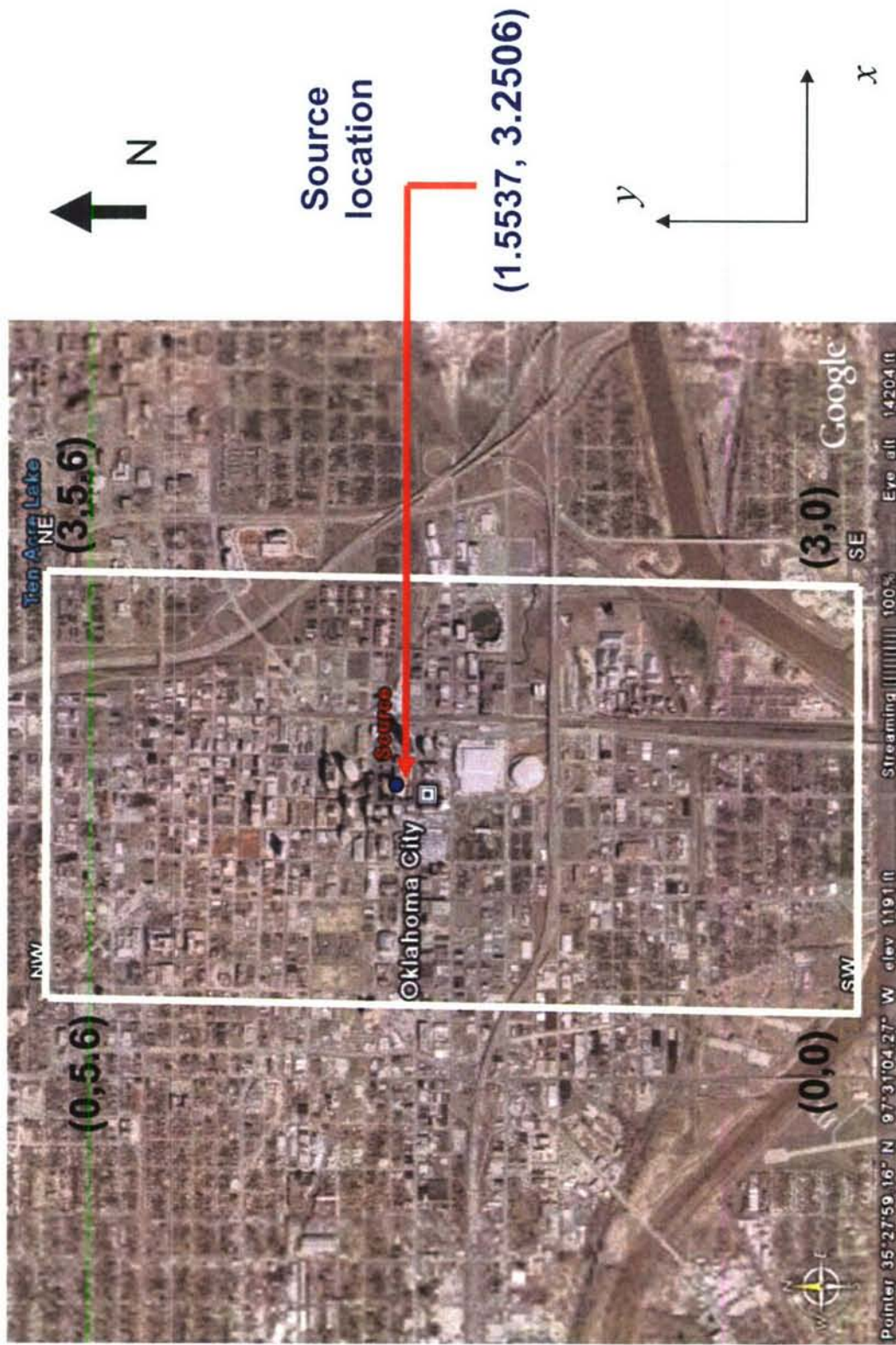


Figure 6. Computational domain used for simulation of flow in Oklahoma City.

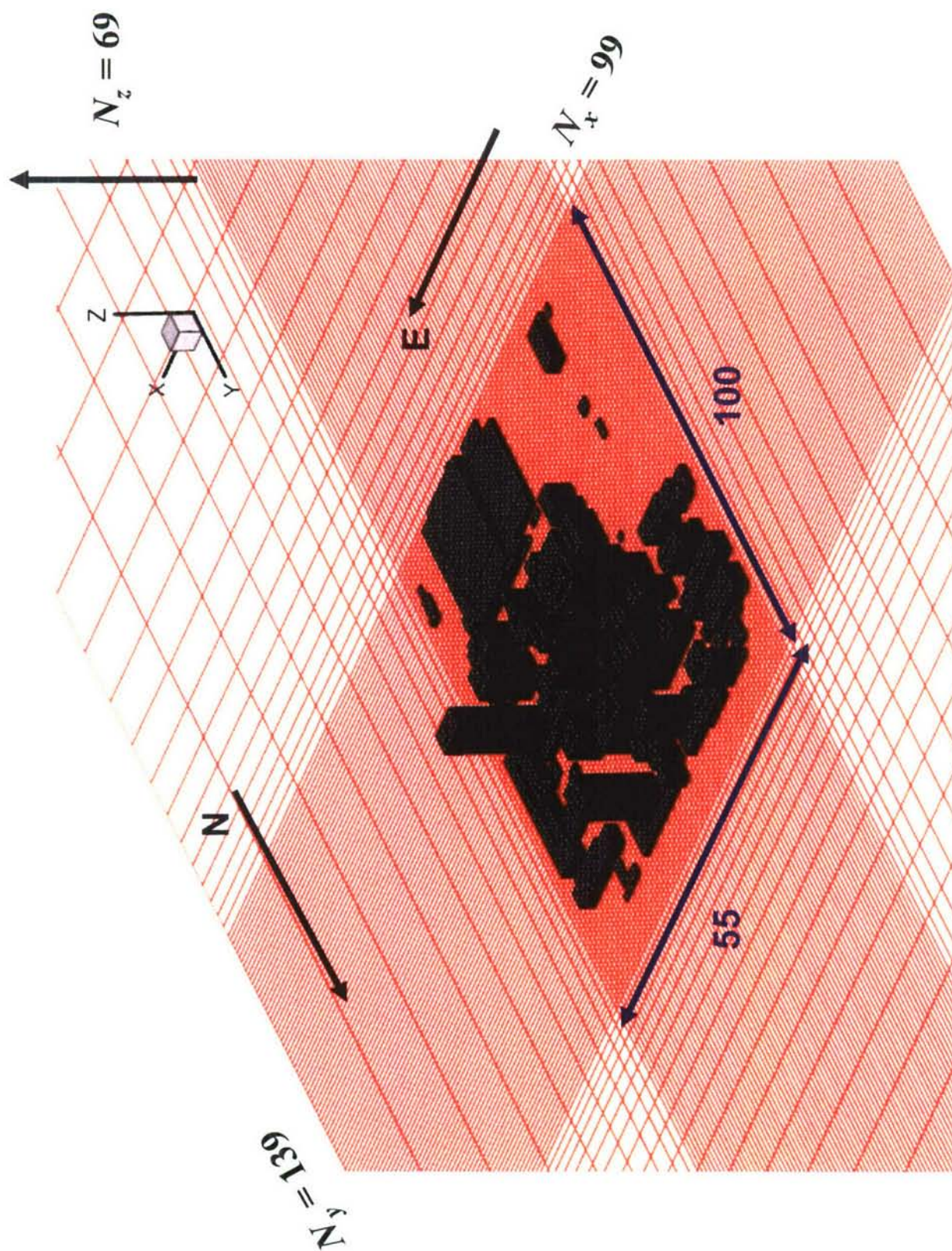
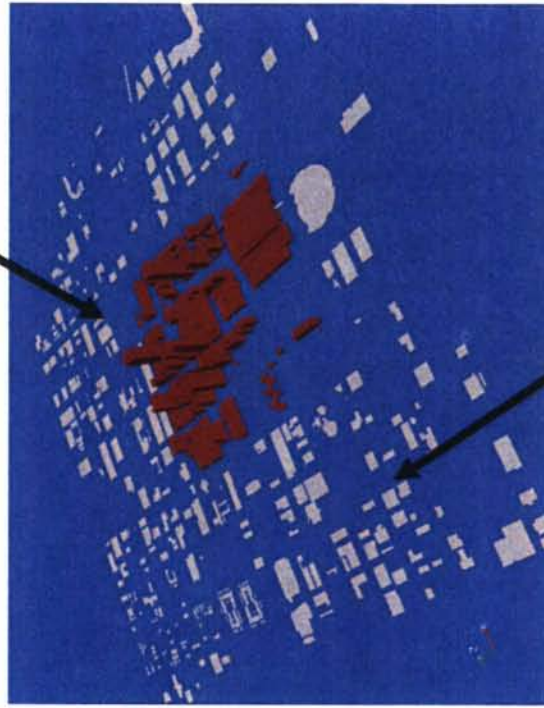


Figure 7. Computational grid generated by urbanGRID for Oklahoma City.

Resolved buildings in building-aware region



Virtual buildings

Figure 8. Satellite photograph of downtown Oklahoma City and 3-D computer rendering of buildings in building-aware region of the computational domain.

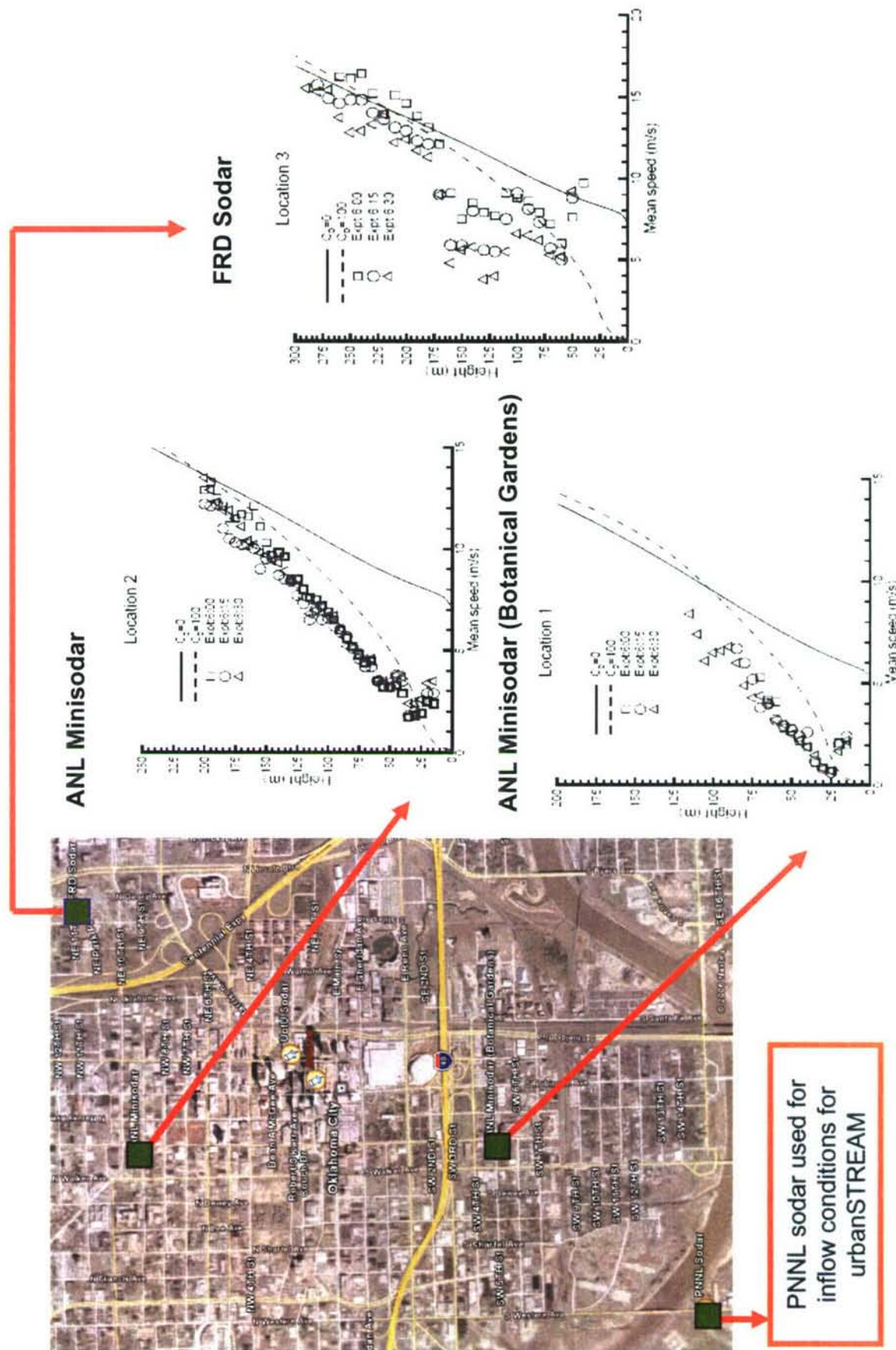


Figure 9. Comparison of mean wind speed measured at three locations in the computational domain with model predictions. The inflow conditions for flow model were obtained from the measurements made by PNNL sodar.



Figure 10. Detectors (squares) were positioned in the CBD sampling grid and at the 1-km sampling arc for measurement of the time-averaged tracer concentrations released from the indicated source (solid circle).

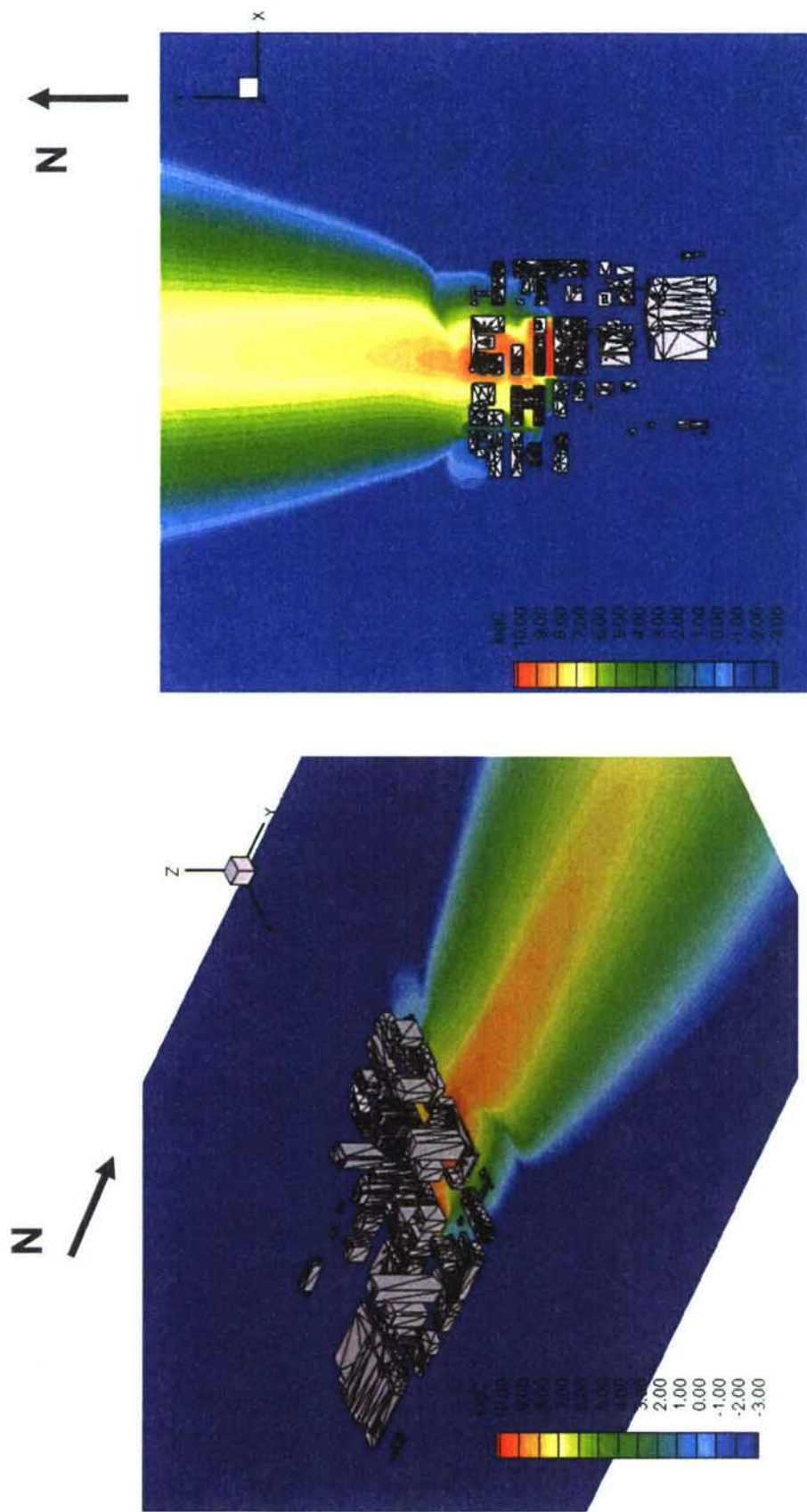


Figure 11. Mean plume concentration isopleths (logarithmic scale) at ground level for tracer release on south side of Park Avenue (Oklahoma City).

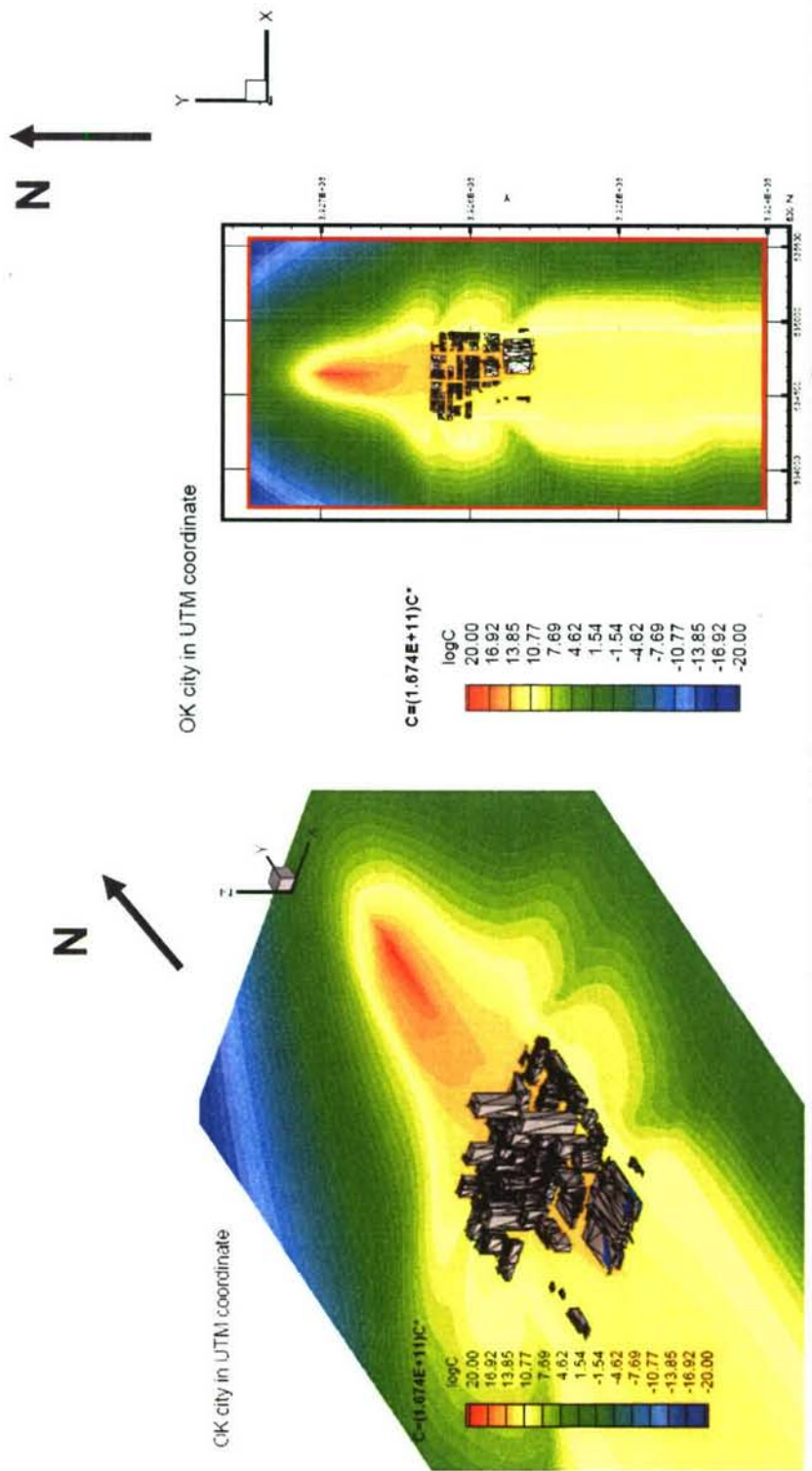


Figure 12. Influence function isopleths (logarithmic scale) at ground level associated with a receptor (#515) at the 1-km sampling arc (Oklahoma City).

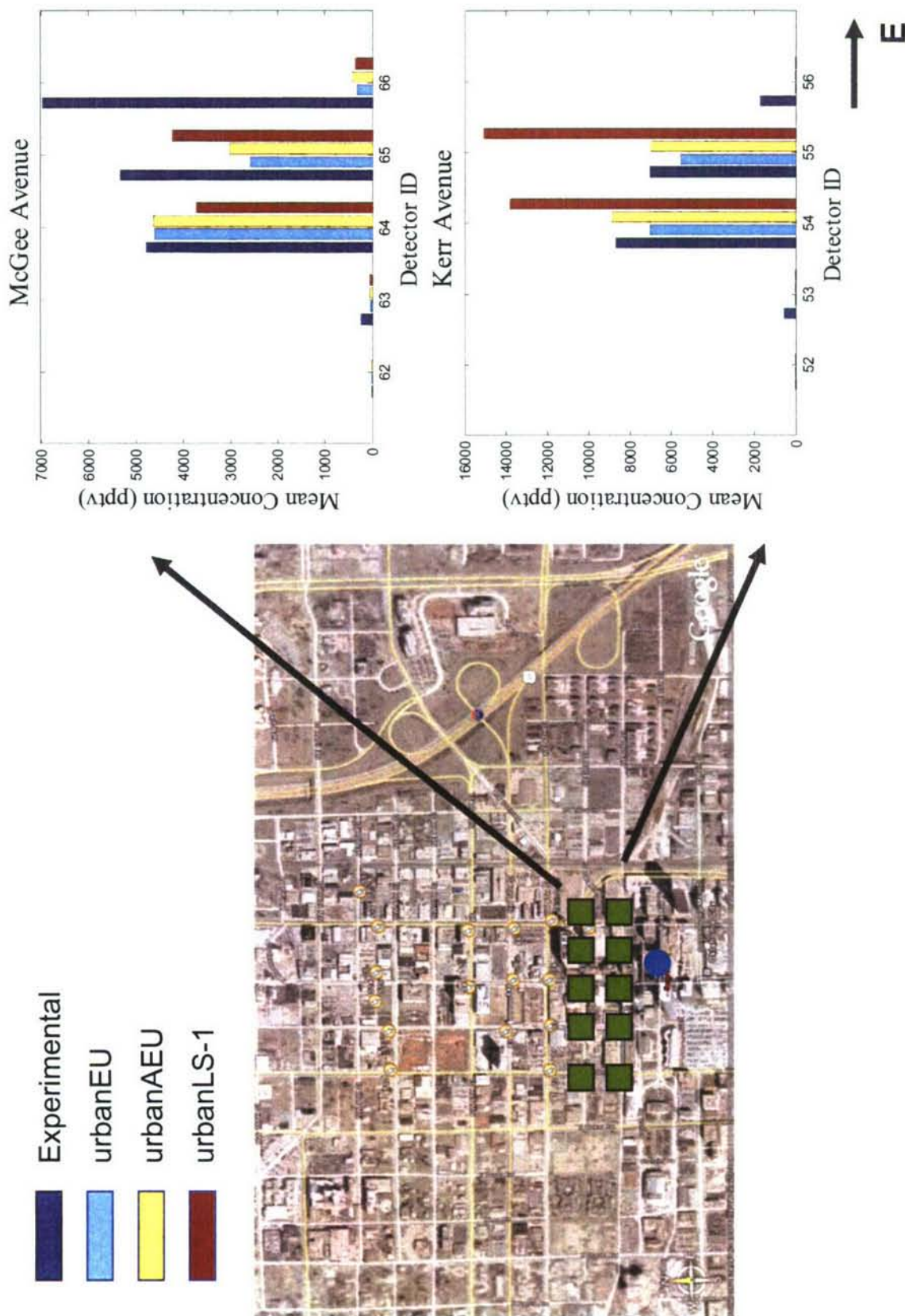


Figure 13. Comparison of predicted mean concentrations obtained from urbanEU, urbanAEU and urbanLS-1 with experimental measurements obtained with detectors along Kerr Avenue and McGee Avenue.

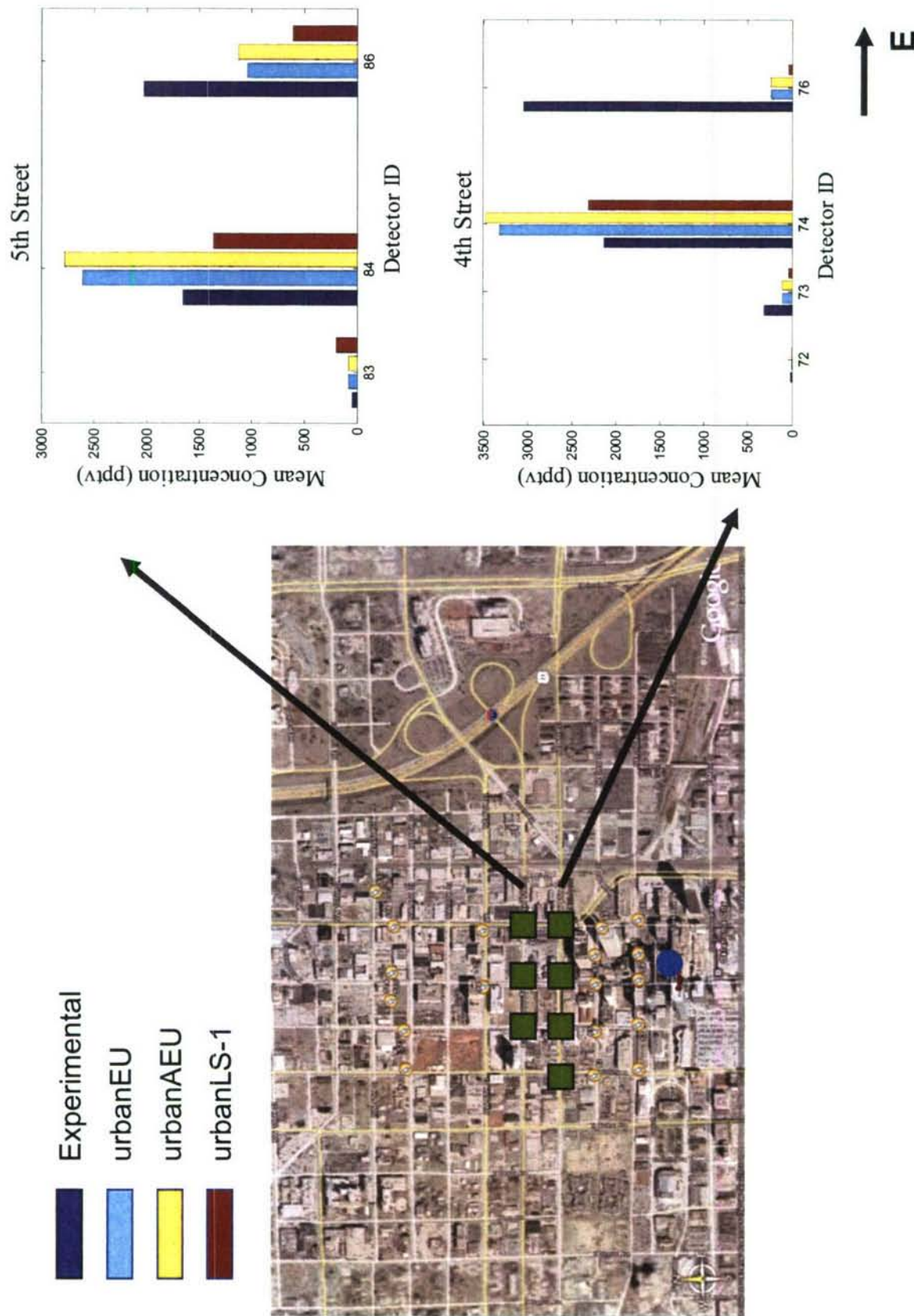


Figure 14. Comparison of predicted mean concentrations obtained from urbanEU, urbanAEU and urbanLS-1 with experimental measurements obtained with detectors along 4th Street and 5th Street.

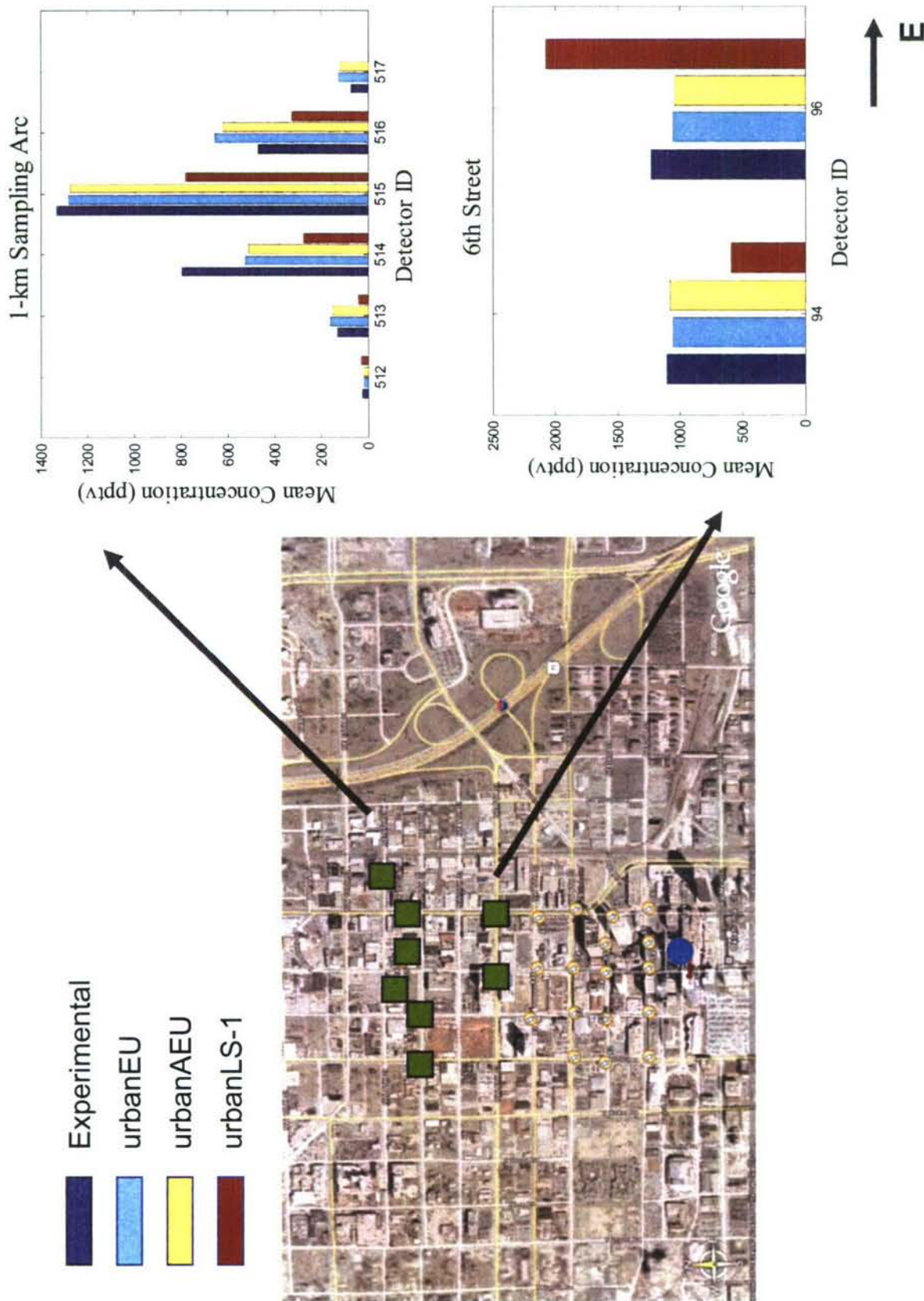


Figure 15. Comparison of predicted mean concentrations obtained from urbanEU, urbanAEU and urbanLS-1 with experimental measurements obtained with detectors along 6th Street and the 1-km sampling arc.

UNCLASSIFIED
SECURITY CLASSIFICATION OF FORM
(highest classification of Title, Abstract, Keywords)

DOCUMENT CONTROL DATA <small>(Security classification of title, body of abstract and indexing annotation must be entered when the overall document is classified)</small>		
1. ORIGINATOR (the name and address of the organization preparing the document. Organizations for who the document was prepared, e.g. Establishment sponsoring a contractor's report, or tasking agency, are entered in Section 8.) Defence R&D Canada – Suffield PO Box 4000, Station Main Medicine Hat, AB T1A 8K6	2. SECURITY CLASSIFICATION (overall security classification of the document, including special warning terms if applicable) Unclassified	
3. TITLE (the complete document title as indicated on the title page. Its classification should be indicated by the appropriate abbreviation (S, C or U) in parentheses after the title). Technical Description of Urban Microscale Modeling System: Component 1 of CRTI Project 02-0093RD		
4. AUTHORS (Last name, first name, middle initial. If military, show rank, e.g. Doe, Maj. John E.) Yee, Eugene, Lien, Fue-Sang, Ji, Hua		
5. DATE OF PUBLICATION (month and year of publication of document) March 2007	6a. NO. OF PAGES (total containing information, include Annexes, Appendices, etc) 55	6b. NO. OF REFS (total cited in document) 19
7. DESCRIPTIVE NOTES (the category of the document, e.g. technical report, technical note or memorandum. If appropriate, enter the type of report, e.g. interim, progress, summary, annual or final. Give the inclusive dates when a specific reporting period is covered.) Technical Report, Final, January 1, 2005 – December 31, 2006		
8. SPONSORING ACTIVITY (the name of the department project office or laboratory sponsoring the research and development. Include the address.) CBRN Research and Technology Initiative		
9a. PROJECT OR GRANT NO. (If appropriate, the applicable research and development project or grant number under which the document was written. Please specify whether project or grant.) CRTI Project No. 02-0093RD	9b. CONTRACT NO. (If appropriate, the applicable number under which the document was written.)	
10a. ORIGINATOR'S DOCUMENT NUMBER (the official document number by which the document is identified by the originating activity. This number must be unique to this document.) DRDC Suffield TR 2007-067	10b. OTHER DOCUMENT NOS. (Any other numbers which may be assigned this document either by the originator or by the sponsor.)	
11. DOCUMENT AVAILABILITY (any limitations on further dissemination of the document, other than those imposed by security classification) (x) Unlimited distribution () Distribution limited to defence departments and defence contractors; further distribution only as approved () Distribution limited to defence departments and Canadian defence contractors; further distribution only as approved () Distribution limited to government departments and agencies; further distribution only as approved () Distribution limited to defence departments; further distribution only as approved () Other (please specify):		
12. DOCUMENT ANNOUNCEMENT (any limitation to the bibliographic announcement of this document. This will normally corresponded to the Document Availability (11). However, where further distribution (beyond the audience specified in 11) is possible, a wider announcement audience may be selected). Unlimited		

UNCLASSIFIED
SECURITY CLASSIFICATION OF FORM

13. **ABSTRACT** (a brief and factual summary of the document. It may also appear elsewhere in the body of the document itself. It is highly desirable that the abstract of classified documents be unclassified. Each paragraph of the abstract shall begin with an indication of the security classification of the information in the paragraph (unless the document itself is unclassified) represented as (S), (C) or (U). It is not necessary to include here abstracts in both official languages unless the text is bilingual).

This report provides a technical description of the models that comprise Component 1 of a 4-year Chemical, Biological, Radiological and Nuclear Research and Technology Initiative (CRTI) Project 02-0093RD entitled "An Advanced Emergency Response System for Chemical Biological Radiological and Nuclear (CBRN) Hazard Prediction and Assessment for the Urban Environment" whose primary objective is the development of an advanced, fully validated, state-of-the-science modeling system for the prediction of urban flow (i.e., turbulent flow through cities) and the concomitant problem of modeling the dispersion of CBRN agents released in a populated urban environment. The principal module of Component 1 is urbanSTREAM, which is a general second-order accurate finite-volume code designed for the simulation of urban flow using a two-equation turbulence closure model (namely, the standard $k-\epsilon$ model and the limited-length-scale $k-\epsilon$ model). Component 1 also incorporates a module (urbanGRID) for the automatic generation of grids in the computational domain when provided with detailed geometric information on the shapes and locations of buildings in the urban environment in the form of Environmental Systems Research Institute (ESRI) Shapefiles. Finally, Component 1 also includes modules for the prediction of urban dispersion in the Eulerian framework: namely, urbanEU which is an Eulerian grid dispersion model based on numerical solution of a K -theory advection-diffusion equation (source-oriented approach) and urbanAEU which is a receptor-oriented dispersion model based on numerical solution of the adjoint of the K -theory advection-diffusion equation. The report describes the current status of the urban microscale flow and dispersion modeling system developed in Component 1 and presents a case study of the application of this system in stand-alone mode to the simulation of flow and tracer dispersion in a real cityscape. The numerical simulations of Intensive Observation Period (IOP) 9 in the Joint Urban 2003 (JU2003) experiments conducted in Oklahoma City, Oklahoma provide an initial demonstration that the developed modeling system can correctly reproduce many features of the flow and dispersion in a real urban environment.

14. **KEYWORDS, DESCRIPTORS or IDENTIFIERS** (technically meaningful terms or short phrases that characterize a document and could be helpful in cataloguing the document. They should be selected so that no security classification is required. Identifiers, such as equipment model designation, trade name, military project code name, geographic location may also be included. If possible keywords should be selected from a published thesaurus, e.g. Thesaurus of Engineering and Scientific Terms (TEST) and that thesaurus-identified. If it is not possible to select indexing terms which are Unclassified, the classification of each should be indicated as with the title.)

Urban Flow Prediction, Urban Dispersion, Computational Fluid Dynamics, Numerical Methods in Fluids, Model Validation

Defence R&D Canada

Canada's Leader in Defence
and National Security
Science and Technology

R & D pour la défense Canada

Chef de file au Canada en matière
de science et de technologie pour
la défense et la sécurité nationale



www.drdc-rddc.gc.ca

